AGU PUBLICATIONS

Geochemistry, Geophysics, Geosystems

RESEARCH ARTICLE
10.1002/2014GC005509

Key Points:
- Higher resistivity with increased coastal plate coupling implies lesser fluid
- Low-resistivity fluid coincides with eclogitization and slow-slip earthquakes
- Resistivity structure of arc melt source reflects slab inputs and state of stress

Supporting Information:
- SegmentationCascadiaMT_ReadMe
- SegmentationCascadiaMT_SupplInfo

Correspondence to:
P. E. Wannamaker,
pewanna@egi.utah.edu

Citation:
Wannamaker, P. E., R. L. Evans, P. A. Bedrosian, M. J. Unsworth, V. Maris, and R. S. McGary (2014), Segmentation of plate coupling, fate of subduction fluids, and modes of arc magmatism in Cascadia, inferred from magnetotelluric resistivity, *Geochem. Geophys. Geosyst.*, *15*, 4230–4253, doi:10.1002/2014GC005509.

Received 18 JUL 2014
Accepted 2 OCT 2014
Accepted article online 14 OCT 2014
Published online 11 NOV 2014

Segmentation of plate coupling, fate of subduction fluids, and modes of arc magmatism in Cascadia, inferred from magnetotelluric resistivity

Philip E. Wannamaker[1], Rob L. Evans[2], Paul A. Bedrosian[3], Martyn J. Unsworth[4], Virginie Maris[1], and R. Shane McGary[2,5]

[1]Energy and Geoscience Institute, University of Utah, Salt Lake City, Utah, USA, [2]Department of Geology and Geophysics, Woods Hole Oceanographic Institution, Woods Hole, Massachusetts, USA, [3]Crustal Geophysics and Geochemistry Science Center, U.S. Geological Survey, Denver Federal Center, Denver, Colorado, USA, [4]Department of Physics, University of Alberta, Edmonton, Alberta, Canada, [5]Department of Physics, The College of New Jersey, Ewing, New Jersey, USA

Abstract Five magnetotelluric (MT) profiles have been acquired across the Cascadia subduction system and transformed using 2-D and 3-D nonlinear inversion to yield electrical resistivity cross sections to depths of ~200 km. Distinct changes in plate coupling, subduction fluid evolution, and modes of arc magmatism along the length of Cascadia are clearly expressed in the resistivity structure. Relatively high resistivities under the coasts of northern and southern Cascadia correlate with elevated degrees of inferred plate locking, and suggest fluid- and sediment-deficient conditions. In contrast, the north-central Oregon coastal structure is quite conductive from the plate interface to shallow depths offshore, correlating with poor plate locking and the possible presence of subducted sediments. Low-resistivity fluidized zones develop at slab depths of 35–40 km starting ~100 km west of the arc on all profiles, and are interpreted to represent prograde metamorphic fluid release from the subducting slab. The fluids rise to forearc Moho levels, and sometimes shallower, as the arc is approached. The zones begin close to clusters of low-frequency earthquakes, suggesting fluid controls on the transition to steady sliding. Under the northern and southern Cascadia arc segments, low upper mantle resistivities are consistent with flux melting above the slab plus possible deep convective backarc upwelling toward the arc. In central Cascadia, extensional deformation is interpreted to segregate upper mantle melts leading to underplating and low resistivities at Moho to lower crustal levels below the arc and nearby backarc. The low- to high-temperature mantle wedge transition lies slightly trenchward of the arc.

1. Introduction

The Cascadia subduction system of western North America upends any notion of subduction being nearly invariant along the strike of an orogen. Earthquake activity and geodetic data point to stronger locking between the Juan de Fuca and North American plates along the subduction interface near the coast in the north below Washington state and Vancouver Island, and to the south in California, but less so in central Oregon [*McCrory et al.*, 2012; *Hyndman*, 2013]. Episodic tremor and slip (ETS) events near forearc Moho or uppermost mantle depths are also concentrated in the northern and southern regions, with a more quiescent central zone under Oregon having slower recurrence intervals [*Brudzinski and Allen*, 2007; *Gomberg et al.*, 2010; *Beroza and Ide*, 2011]. The Cascades volcanic arc is partitioned along strike petrologically and structurally with increasing degrees of inferred subducted plate input and Basin and Range extensional overprint southward into Oregon and northeastern California [*Hildreth*, 2007; *Schmidt et al.*, 2008]. The physicochemical states at depth that represent the driving factors behind surface observations have been interpreted to date largely on the basis of seismology, geodesy, structural geology, and volcanic petrology. However, much ambiguity remains regarding the relative roles of fluids, sediments and temperature in plate mechanical behavior. Models for fluid release or melt generation during subduction merit validation or refinement through new geophysical images and interpretation.

High-quality magnetotelluric (MT) data have been collected in the Pacific Northwest region, especially during the past decade to the point where new or complementary inferences are possible regarding key

subduction processes and their variations along Cascadia. In this paper, we present and compare results of five MT land transects from the coast across northwest Washington (CAFE-MT), northwest Oregon (EMSLAB), southwest Oregon (SWORMT), and northwest California (Klamath-Modoc), and finally Vancouver Island and southwest British Columbia (ABCS) (Figure 1). The data have sufficient bandwidth in most cases to construct models of electrical resistivity (or its inverse, conductivity) from depths of a few 100s m to >200 km. Using external constraints, inferences from the models are made regarding fluids and sediments subducted down the trench, whether temperature alone or also fluids influence the extent of plate locking in the subduction shear zone, conditions of dehydration reactions and the movement of fluids liberated in the oceanic plate, the relation of ETS to imaged fluid formation, how released subducted fluids approach the volcanic arc, and whether petrologic models of the variation in melting conditions along the arc are supported by images of resistivity. Coarser-scale but fully 3-D views of resistivity beneath the Cascadia system derived from the Earthscope MT Transportable Array data [*Bedrosian and Feucht*, 2014; *Meqbel et al*., 2014] provide valuable constraints and context for the focused views we offer here.

2. Geologic Background

The processes of subduction and arc magmatism along the Cascadia system have diverse manifestations that reflect numerous mechanisms. Important factors concern plate coupling, exsolution of slab fluids, and pressure-temperature-composition-strain controls on melt geometries. We review these briefly below to the extent they may bear on resistivity structure.

2.1. Regional Tectonic Setting

The present Cascadia subduction system and volcanic arc was established ~40 Ma with disappearance of the Farallon plate and development of the Juan de Fuca plate [*Humphreys*, 2008]. In middle Cenozoic time, the arc extended farther south to present day southwestern Nevada but has shortened northward with migration of the Mendocino triple junction, formation of a growing slab window, and growth of the San Andreas-Walker Lane strike-slip fault systems [*Wilson et al*., 2005; *Faulds and Henrys*, 2008; *Colgan et al*., 2011; *Busby*, 2013]. Mesozoic and Paleozoic metamorphic, volcanic, and plutonic basement blocks underlie the Cascadia backarc regions and, in northern California and southern Oregon (Klamath terrane), much of the forearc as well [*Wright and Wyld*, 2006; *Dorsey and LaMaskin*, 2007; *Dickinson*, 2008; *Blakely et al*., 2011] (Figure 1). The Siletz volcanic terranes were accreted in the early Cenozoic and lie beneath the forearc and arc from north-central Oregon through Washington to southernmost Vancouver Island where it is named the Crescent terrane [*Wells et al*., 2014]. For an alternate view extending Siletz rocks under more of the backarc of central Cascadia, see *Humphreys* [2008]. Vancouver Island and southwesternmost British Columbia (B.C.) are floored mainly by the Wrangellia composite terrane, comprising Paleozoic-Mesozoic metavolcanics sutured to the prior mainland just east of the modern arc [*Monger and Price*, 2002].

An exceptional thickness of Juan de Fuca subduction mélange rocks progressively accreted since Eocene time underlies northwesternmost Washington including the Olympic Mountains of [*Parsons et al*., 1995] (Figure 1). Basement below coastal northwestern California is late Mesozoic to early Cenozoic Franciscan and Coastal Belt mélange [*Ernst*, 2011]. The U.S. Cascadia backarc as a whole now is extensively covered by late Tertiary Columbia River or High Lava Plains basalt flows. Clockwise block rotation of the Cascades about a pole in northeastern Oregon from Miocene to present [*McCaffrey et al*., 2013] produces oblique compression in the northern Cascades spawning the backarc Yakima fold and thrust belt [*Blakely et al*., 2011] (Figure 1). In central Cascadia, rotation and slab rollback produce a net effective migration of volcanism eastward by ~75 km leaving behind a remnant plutonic Western Cascades [*Wells and McCaffrey*, 2013]. Backarc southeastern Oregon and northeastern California experienced oblique extensional to strike-slip faulting during this time as Great Basin extension encroached. This includes the prominent Cascades graben running much of the length of Oregon [*Humphreys*, 2008; *Schmidt et al*., 2008].

2.2. Subducted Plate Properties

The Cascadia subduction system is regarded as a thermal end-member, featuring the consumption of a young, hot plate [e.g., *van Keken et al*., 2011]. The subducting Juan de Fuca plate has an age varying between 7 and 9 Ma at the trench offshore Washington and Oregon, whereas the plate formed at the Gorda ridge is slightly younger (5–7 Ma) at the trench offshore northern California [*Schmidt et al*., 2008].

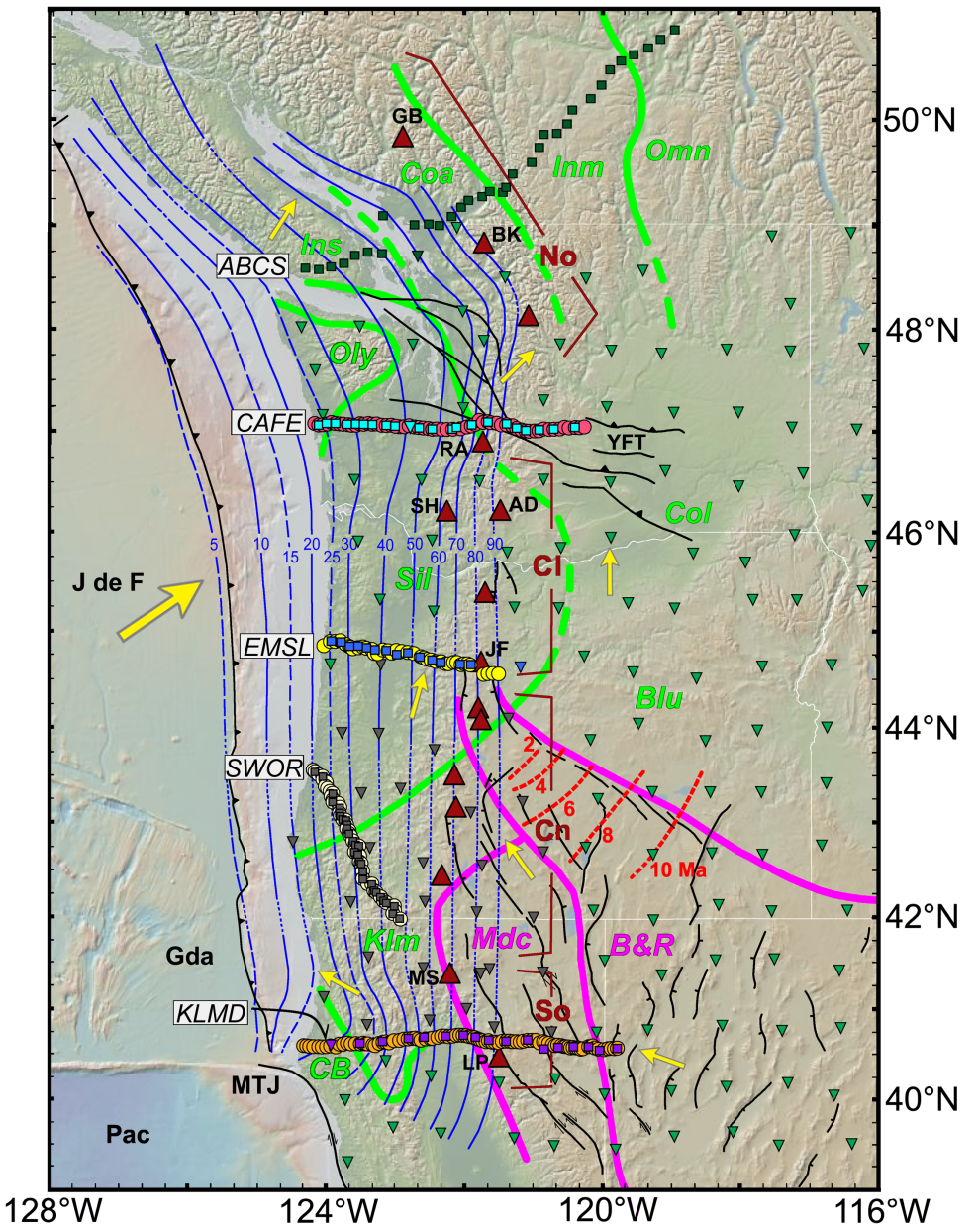

Figure 1. Location map for four profiles of MT soundings analyzed herein (ABCS, CAFE, EMSLAB = EMSL, SWOR = SWORMT, Klamath-Modoc = KLMD). Round site symbols refer to wideband (WB) stations whereas square symbols refer to long period (LP) stations. The Earthscope USArray LP MT stations are inverted medium green triangles, whereas the occasional Earthscope station used in a profile inversion is recolored according to the other LP stations of that profile. Gray Earthscope stations were used in the 3-D inversion of the SWORMT data. Yellow GPS geodetic motion estimate and Juan de Fuca convergence arrows are after *Wells and McCaffrey* [2013]. Central and southern Cascade Range and Basin and Range area normal faults are in black with stick on downthrown side [*Hildreth*, 2007; *Stewart and Carlson*, 1978]. Contours of rhyolitic volcanism in southeast Oregon approaching the central Cascades are red dashes [*Hildreth*, 2007]. Yakima fold and thrust belt (YFT) faults northeast of Mount Rainier are simplified from *Blakely et al.* [2011]. Green bands enclose terranes Siletz (Sil), Klamath (Klm), Blue Mtns (Blu), Insular (Ins), B.C. Coastal Belt (Coa), Intermontane (Inm) and Omineca (Omn) [*Monger and Price*, 2002; *Humphreys*, 2008; *Schmidt et al.*, 2008]. Eastern boundary of Siletz in Oregon is obscure, but is placed some distance east of arc based upon *Schmidt et al.* [2008]. Olympic Mountains is Oly, Columbia Embayment is Col, and California Coastal Belt is CB. Pink bands enclose actively extensional terranes Basin and Range (B&R) and Modoc Plateau (Mdc). Volcanic chain segment boundaries North (No), Columbia (Cl), Central (Cn), and South (So) are after *Schmidt et al.* [2008]. Mount Garibaldi is GB, Mount Baker is BK, Mount Rainier is RA, Mount St Helens is SH, Mount Adams is AD, Mount Jefferson is JF, Mount Shasta is MS and Lassen Peak within the Lassen Volcanic Center is LP. Plate contours are in blue and are hand-contoured values from *McCrory et al.* [2012]. Offshore, J de F is Juan de Fuca plate, and Gda is Gorda plate (southern Juan de Fuca). DEM base layer is from GeoMapApp utility.

Table 1. List of Geographic and Subduction Process Acronyms Used in Text, Ordered Alphabetically

Acronyms	Geographic/Structural
LP	Long-period MT sounding
LVC	Lassen Volcanic Center
SWCC	Southwest Washington Cascades Conductor
TA	Earthscope Transportable Array
WB	Wideband MT sounding
WRZ	Western Rainier Seismicity Zone
Acronyms	**Process**
ACMA	Average Current Mantle Adiabat
DLP	Deep Long-Period Earthquakes
ETS	Episodic Tremor and Slip
FMC	Forearc Mantle Corner
LFE	Low Frequency Earthquakes
LVL	Low Velocity Layer (S-wave)
NVT	Non-Volcanic Tremor

Subduction dip is somewhat shallower under Washington and southwestern British Columbia than under Oregon, and the width of plate locking (including transition zones) below Washington and Vancouver Island is the greatest of Cozzens [*McCrory et al*., 2012; *Hyndman*, 2013; *Schmalzle et al*., 2014]. *Cozzens and Spinelli* [2012] suggested that hydrothermal circulation in the ocean floor could depress Juan de Fuca plate geotherms and thus widen a thermally controlled locking zone. However, substantial seafloor sedimentary cover is argued to limit circulation offshore Cascadia [*Hasterok et al*., 2011; *Hyndman*, 2013] and the breadth of locking off northern Cascadia has been related to shallow plate dip [*McCrory et al*., 2012]. Marine seismic reflection surveys imply landward thrust vergence with essentially all oceanic sediment offscraped at the trench offshore Washington so that little enters the subduction zone [*Flueh et al*., 1998].

Complete sediment offscraping does not appear to occur offshore Oregon. Seismically imaged seaward thrust fault vergence and decreased P-wave velocities suggest the presence of a subduction sediment channel ~1 km in thickness under the coast [*Gulick et al*., 1998; *Trehu et al*., 2012; *McNeill et al*., 2013]. Sediment compaction and clay dehydration can release large amounts of fluids to distances approaching 100 km from the trench [*Saffer and Tobin*, 2011]. Coincidentally, the plate locking width appears to be narrowest along Oregon, barely reaching onshore if at all [*Gomberg et al*., 2010; *Hyndman*, 2013; *Schmalzle et al*., 2014]. The locked plus transition zone width increases again in northern California [*Gomberg et al*., 2010; *Schmalzle et al*., 2014] accompanied by high seismicity in both upper and lower plates, in contrast to forearc seismicity beneath Oregon [*McCrory et al*., 2012]. The plate here is substantially warped in concert with N-S compression between the southern Juan de Fuca and Pacific plates across the Mendocino triple junction, and possesses a much shallower dip than elsewhere in Cascadia to a distance of ~75 km inland from the coast (Figure 1). Thrusts mostly are landward vergent but *Gulick et al*. [1998] concluded that a few hundred meters of ocean sediment may be subducted beneath northern California.

Data from dense passive seismic arrays across northern Oregon, Washington, and Vancouver Island show dipping layers of low S-wave velocity (LVL) and high V_P/V_S in the 20–45 km depth range where overlain by continental crust [*Audet et al*., 2010; *Bostock*, 2013] (for a list of acronyms, see Table 1). The layers imply fluid overpressures interpreted to reflect low-grade hydrous mineral breakdown and perhaps basalt pore and fracture collapse primarily in the upper oceanic crust [*Saffer and Tobin*, 2011]. The dipping LVL loses coherency and becomes diffuse downdip at a depth of 35–40 km. That is the approximate depth of onset of voluminous dehydration during progressive eclogite formation [*Peacock*, 2009; *Van Keken et al*., 2011; *Bostock*, 2013], suggested to enhance permeability and allow upward escape of fluids. Continuum mechanical models also suggest that in a warm plate such as Juan de Fuca, dehydration fluids released as deep as ~60 km may migrate obliquely upward toward the forearc mantle corner (FMC, or wedge tip) [*Furukawa*, 2009]. Ascending fluid flux is believed responsible for extensive serpentinization of the mantle wedge, producing a reduction in its velocity, and thus substantially obscuring the overlying seismic Moho [*Bostock*, 2013]. Serpentinization also is invoked to explain patterns of forearc magnetization in Cascadia and elsewhere [*Blakely et al*., 2005].

2.3. Episodic Tremor and Slow Earthquakes

Where imaged in northern and central Cascadia, episodic nonvolcanic tremor and slow-slip or low-frequency earthquakes (NVT-LFE or ETS) occur near the downdip limits of the LVLs [*Wech et al*., 2009; *Gomberg et al*., 2010]. The resemblance of this tremor to that seen in volcanic regimes is compatible with fluid movement, as are the migration rates of tremor swarms along the strike of Cascadia. Tremor is vigorous in northern Cascadia and plentiful also under northern California, with north-central Oregon being relatively subdued [*Beroza and Ide*, 2011], in some correlation with plate locking. There appears to be a gap of ~50 km width between the downdip reach of plate locking and the band of tremor in Cascadia [*McCrory*

et al., 2014]. Tremor event depths are difficult to pinpoint due to first arrival uncertainties, but the band appears laterally confined to where depth to the Juan de Fuca plate interface lies in the 30–45 km range [*Boyarko and Brudzinski*, 2010; *McCrory et al*., 2014]. Based on results from the densely instrumented Japanese system and more limited results from northernmost Cascadia, there has been a presumption that tremor events lie near the plate interface [*Royer and Bostock*, 2014].

Further highlighting system segmentation, ETS tend to concentrate in northern and southern Cascadia [*Boyarko and Brudzinski*, 2010; *Beroza and Ide*, 2011]. The average recurrence interval of ETS varies markedly, with an interval of ~14 months in the north, 19 months in central Cascadia, and 11 months in the south [*Brudzinski and Allen*, 2007]. Typical inferred LFE displacements of 1–2 cm and their modulation by tides and occasional triggering by distant earthquakes imply very low stress drops, evidently placing them close to the onset of stable sliding along the subduction interface [*Gomberg et al*., 2010]. One interpretation considers stable sliding as mainly thermally controlled, occurring at temperatures above 450°C, and perhaps enabled also by formation of low-friction talc at the mantle-oceanic plate interface during serpentinitization of the mantle [*Hyndman*, 2013]. However, high fluid pressures also may induce slip by creating low effective normal stresses [*Sibson*, 2007]. At present, the most precisely located LFE are those under the CAFE and Vancouver Island areas, determined using sophisticated waveform correlation and clustering techniques [*Royer and Bostock*, 2014]. The LFE group in the 35–40 km depth range near the estimated plate interface [*McCrory et al*., 2012] and the FMC.

A characteristic distance in Cascadia from the downdip limit of ETS to the arc volcanism is ~100 km, or about one-half the width of the onshore forearc. Over this deeper interval, the pathways and fate of fluids released during subducted plate dehydration are obscure. With a young, warm subducted plate, most of the hydrous minerals are expected to have broken down before reaching depths below the arc [*Van Keken et al*., 2011]. Farther inland from the dipping LVL, S-wave structure becomes diffuse and difficult to ascribe, although some S-wave features are interpreted to reflect deeper fluid migration [*McGary et al*., 2014].

2.4. Arc Volcanic Variations

Substantial along-strike variations exist in the arc volcanic and tectonic style of the Cascadia subduction zone [*Leeman et al*., 2005; *Hildreth*, 2007; *Schmidt et al*., 2008]. Despite high visibility stratovolcanoes such as Mount Rainer or Mount Shasta, volcanism here is fundamentally basaltic. Traditionally, slab inputs to Cascades volcanism were considered somewhat limited, especially for the northern segment (Figure 1), in keeping with subduction of a young Juan de Fuca plate and relatively rapid dewatering. More recently, *Grove et al*. [2012] argue that peridotitic chlorite may persist to ~800°C and thus provide water for H_2O-rich melting near subarc plate depths. Water contents of primary melts observed at the surface reflect melt volume increases and water dilution as near-slab melts rise through the hotter mantle wedge.

Degree of slab contribution and flux melting appear to increase southward to a maximum for Mount Shasta and Lassen Volcanic Center (LVC) areas [*Schmidt et al*., 2008] (Figure 1). Subduction-related input may be both modern, from a relatively deformed Gorda plate segment, or ancient from lithospheric mantle of Klamath-Sierran age. The hottest and driest low-potassium magmas are seen in the central (Oregon) Cascadia segment from Mount Adams southward, and are suspected to be related to extensional overprint related to Basin and Range encroachment [*Leeman et al*., 2005; *Hildreth*, 2007; *Schmidt et al*., 2008].

Crustal extension is seen in the southern Cascadia segment as well in the Modoc Plateau, but to a lesser degree, and faulting involves a more strike-slip component (Figure 1). Across the Modoc Plateau to the edge of the Great Basin at the California-Nevada border, one encounters the southern end of a late Miocene and younger High Lava Plains basaltic trend (Shin Mountain-Storm Mountain cones) described by *Till et al*. [2013]. These volcanic units are interpreted to have formed through adiabatic mantle upwelling driven by subduction corner flow at depths just below the Moho.

3. MT Transect Resistivity Models

The results and interpretation of the MT transects are presented individually, beginning with the U.S. profiles (Figure 1) because of their relatively high data sampling and resolution. In the main text, we present final resistivity models, describe principal features, assign physicochemical causes or states to resistivity structures, and integrate with independent geological, geophysical, and geochemical constraints. A brief

review of the MT method, detailed displays of the MT data in pseudosection format, geoelectric strike analyses, construction of regularized inversion models, and sensitivity tests of some key model features, are presented in the supporting information.

We then compare features along profiles in terms of resistivity character as well as ancillary geophysics, structure, and petrology to show how resistivity corroborates or may refine existing models of processes within the Cascadia subduction system. The recently analyzed CAFE and EMSLAB profiles [*Evans et al*., 2014; *McGary et al*., 2014] are combined with new MT data from southern Cascadia (KLMD profile) plus a reanalysis of MT data across southwestern Oregon (SWORMT profile) [*Bedrosian and Box*, 2007] and southwestern B.C. (ABCS profile) [*Soyer and Unsworth*, 2006; *Rippe et al*., 2013]. All are jointly interpreted in terms of a range of processes from subcoastal conditions to the subduction backarc and how the processes change along strike of the system.

3.1. CAFE-MT Profile, Washington

Our line in Washington coincides with the E-W swath of passive seismic stations of the CAFE experiment [*Abers et al*., 2009], which is here denoted CAFE-MT, and crosses the Columbia arc segment. There are 60 wideband (WB) and 19 long-period (LP) stations (see supporting information) collected in 2009 and 2010 over a total period range from 0.005 s to as long as ∼10,000 s at some sites. The profile length is ∼300 km and the average station spacing is ∼5 km. The data were transformed with a 2-D nonlinear inversion to produce an electrical resistivity cross section (see supporting information Figures S1–S5) plotted with annotation in Figure 2. In this paper, however, we do not impose constraints upon the geometry or resistivity of the downgoing slab, as was done previously [*Evans et al*., 2014; *McGary et al*., 2014], in order to offer an interpretation based on the MT data alone.

The model shown in Figure 2 contains a low resistivity layer deepening from just inland of the coast to a distance of ∼75 km. We equate this conductor to fluids distributed along the plate interface [drawn from *McCrory et al*., 2012] generated by low-grade dehydration reactions and perhaps pore fluid collapse in altered oceanic crust. At the updip end lies a compact conductor above the plate interface 10–25 km inland of the coast. This appears likely to be a package of mid-Tertiary accreted oceanic sediments backstopped against Siletz terrane (Crescent Formation) igneous rocks; the correspondence with the lithologic boundary as imaged from wide-angle seismic data by *Parsons et al*. [1995] is close. Why this package should be particularly conductive is unclear as these would not be young oceanic sediments but perhaps as old as Eocene. However, MT data and modeling by *Aprea et al*. [1998] ∼70 km to the north across the Olympic Mountains and Puget Lowlands also showed that these accreted sediments are of low resistivity as far east as the boundary with the Siletz terrane.

A significant feature of the model is the lack of a low-resistivity layer under and just on land from the coastline, and also offshore toward the trench. This is seen in the model of *McGary et al*. [2014] as well. As tested with supporting information Figures S6 and S7, low MT impedance phase response signifies that this region must remain moderately resistive implying low amounts of interconnected conducting fluids or sediments. In turn, a lack of fluids to promote low stress deformation should enable seismic energy buildup. This may be reflected in the relatively high observed seismicity and could contribute to enhanced plate locking at this latitude. We believe this conclusion is corroborated in our comparison to structure under the EMSLAB and Klamath-Modoc profiles discussed below. However, the situation may be more complex for the upcoming SWORMT line where offshore plate locking appears to increase again while seismicity remains low.

At a distance of ∼75 km inland and a depth of ∼40 km, the low-resistivity layer becomes more pronounced and begins with greater distance to depart from the plate interface (Figure 2). Modeled temperatures along the interface at this position should be 500–550°C [*Peacock*, 2009; *Syracuse et al*., 2010] which would correspond to breakdown of amphibolite facies hydrous minerals to release free, aqueous fluids. This process has been termed eclogitization by others [e.g., *Rondenay et al*., 2001, 2008]. The increase here in conductance (integrated thickness/resistivity) of this layer commences near the loss of coherence of S-wave velocity structure cited previously [*Abers et al*., 2009; *Bostock*, 2013] and near LFE precisely located by *Royer and Bostock* [2014] (Figure 2). Most tremor (NVT) lies arcward of the inferred eclogitization and LFE. The eclogitization commences trenchward of the FMC where the Moho (40 km, from *Bostock* [2013]) meets the subduction interface [*McCrory et al*., 2014]. Serpentinization of the mantle wedge tip by fluids is not believed responsible for the low resistivity as laboratory measurements of serpentine have yielded high resistivity

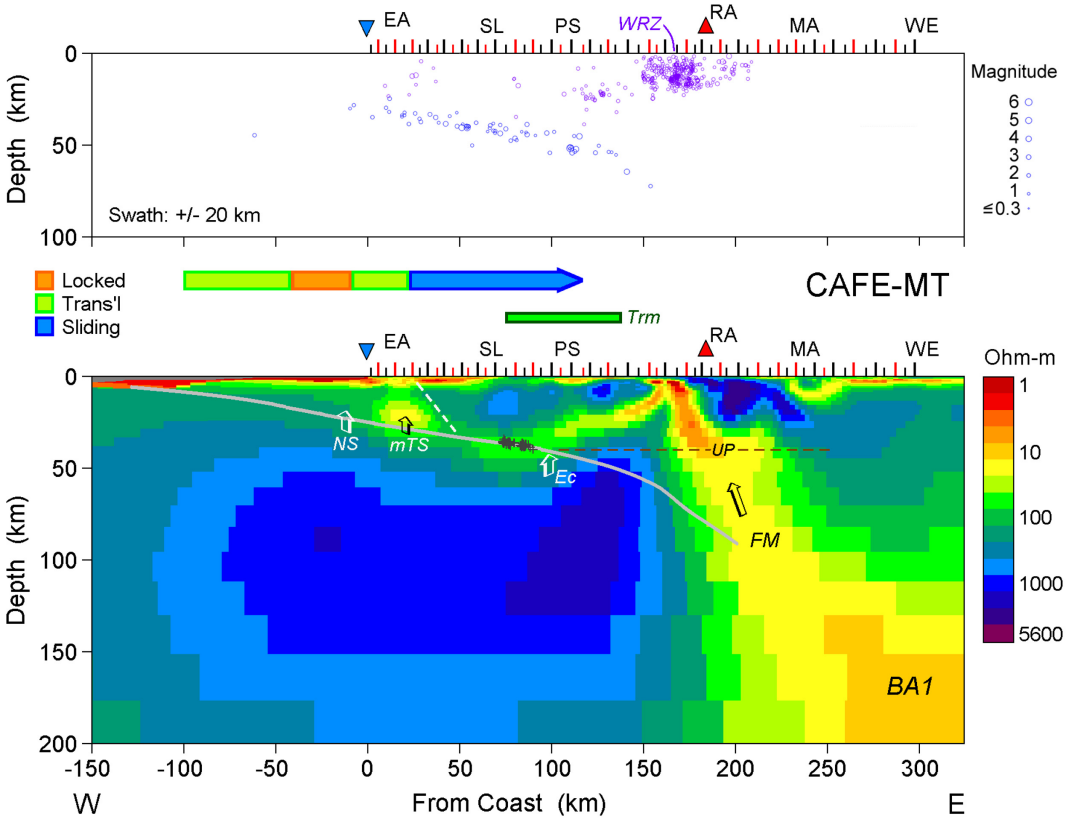

Figure 2. (bottom) Two-dimensional nonlinear inversion resistivity model from MT data along the CAFE transect as described in supporting information. No vertical exaggeration. Red ticks denote MT site locations with both WB and LP instruments, whereas black ticks denote WB only. Physiographic features are Eocene accreted material (EA), Siletz exposure (SL), Puget Sound (PS), Mount Rainier (RA), Manastash Ridge (MA), and Wenatchie Ridge (WE). Inverted blue triangle is coastline and seawater wedge is gray. Subducted plate interface follows *McCrory et al.* [2012]. Sloping dashed line toward coast is possible accretion-Siletz contact area. LFE locations (dark gray plus) are in a ±20 km swath from *Royer and Bostock* [2014]. Abbreviations in bottom plot include no sediments (NS), mid-Tertiary sediments (mTS), magmatic underplating (UP), subduction flux melting (FM), and backarc upwelling 1 (BA1) corresponding to that of *Meqbel et al.* [2014]. Eclogitization (Ec) up-arrow drawn near end of S-wave LVL coherency [*Bostock*, 2013]. (top) Seismicity in denoted swath from *McCrory et al.* [2012] partitioned into lower plate (blue) and upper plate (lavender) events. Large colored horizontal arrow in middle represents width of locked (>70%), transitional (15–70%) and steady sliding (<15%) interplate coupling according to Gaussian decadal-scale slip model of *Schmalzle et al.* [2014]. Horizontal dark green box denotes lateral extent of tremor (Trm) shown by *McCrory et al.* [2014]. Horizontal-dashed red-brown line at 40 km depth is Moho from *Bostock* [2013].

values [*Guo et al.*, 2011; *Reynard et al.*, 2011]. We thus believe the resistivity structure further implicates fluids in defining the transition to steady sliding between the upper and lower plates through rock weakening.

Farther inland, the low-resistivity layer shallows and increases in conductance toward the arc. An obvious possible explanation is that the layer represents additional fluids liberated from the oceanic plate that have risen buoyantly to varying levels in the crust. This is in keeping with the expectation that plate hydrous minerals are solid solutions that should break down over finite temperature intervals [*Peacock*, 2009]. Moreover, toward greater depths in the subduction zone, serpentine and chlorite in the uppermost mantle of the subducted plate and in the immediately overlying mantle wedge from prior rehydration by plate fluids should break down progressively and yield fluid as the arc is approached [*van Keken et al.*, 2011].

Global surveys of electrical conductivity in tectonically active regimes [*Hyndman et al.*, 1993; *Wannamaker et al.*, 2008] imply that the tops of such layers typically are thermally controlled along an isotherm in the 350–500°C range depending upon composition (quartz-rich to dioritic). The shallowing of the layer eastward thus may imply upward advection of heat by fluids and forearc melts into the crust not reflected in solid-state thermal models [cf., *Peacock*, 2009]. This is difficult to corroborate independently given the sparse heat flow data in the vicinity of CAFE [*Ingebritsen and Mariner*, 2010]. However, at the shallowest reaches of the low resistivity just west of Mount Rainier, the fluids likely have broken through into the brittle crustal domain in a fault fracture mesh [cf., *Cox*, 2005; *Sibson*, 2007].

Volume of fluids in the low resistivity layer is not easy to constrain given uncertainties in the geometry of interconnection and fluid composition; here we simply offer a lower bound. High salinity fluids at these temperatures are very conductive (>100 S/m) [*Nesbitt*, 1993], and if interconnected efficiently in grain-edge tubules [e.g., *Grant and West*, 1965] ideally require contents of only <0.2 vol % to explain resistivities of 10–30 ohm-m. Although the fluids initially released from the slab are believed to be of low salinity, fluid solute content should increase during passage upward through warmer, less hydrated wedge material [*Reynard et al*., 2011; *Kawamoto et al*., 2014]. At 600°C (or presumably lower temperatures), characteristic residence times of this fluid content may exceed 10 Myr [*Frost and Bucher*, 1994; *Wannamaker*, 2000], allowing persistence of such a low-resistivity layer especially given replenishment from greater depths. Moreover, compressive state of stress in the forearc promotes fluid retention through subhorizontal fissuring [*Sibson*, 2007]. Along the deeper subduction interface from ~100–175 km, the oceanic crust appears resistive (see supporting information tests with Figures S8 and S9) implying lack of significant conductive fluids and correlating with the absence of coherent S-wave structure.

Beneath the arc and backarc areas is a steep and pronounced low-resistivity zone (Figure 2) which extends from a few kilometers depth near Mount Rainier to the estimated slab surface of *McCrory et al*. [2012], and to considerable depths beyond to the east where plate projections are poorly constrained. This structure is quite similar to that resolved using an independent inversion code by *McGary et al*. [2014]; they also showed that it was possible to impose the low resistivity to lie entirely above the slab surface and still achieve a good fit. This structure represents the subduction flux melting zone and the pathways of melt toward the surface, to which we return later. At upper crustal levels, the steep conductor projects slightly west of Mount Rainier where it converges with the rising conductor assigned to continuously liberated fluids from the slab surface. This slight westward shift relative to the arc is not troubling; our profile passes some 20 km north of the volcano. A local NW-SE trend of Pliocene-Quaternary arc intrusive bodies lies through here [*duBray and John*, 2011], possibly influenced by faulting of the Yakima fold-and-thrust belt, and intersects our profile at this location. Moreover, the thick high resistivities in the crust immediately backarc of Mount Rainier suggest a competent block of Paleozoic-Mesozoic metamorphic and plutonic rocks [*Blakely et al*., 2011] which may influence fluid and magma upwelling pathways.

The steeply converging forearc and arc conductors meet just west of the projection of Mount Rainier, coinciding with the northern tip of the large Southwest Washington Cascades conductor (SWCC). The SWCC was discovered in groundbreaking MT measurements by *Stanley et al*. [1990] and confirmed by *Egbert and Booker* [1993] with geomagnetovariation arrays. It has been debated therein whether the SWCC is primarily is due to modern magmatic-hydrothermal processes or instead represents a deeply underthrust sedimentary package of Late Cretaceous to early Eocene age trapped by collision of the Siletz terrane against the prior North American margin [cf., *Hill et al*., 2009]. The dual conductor we resolve appears to correspond to the bilobate SWCC depiction in *Stanley et al*. [1996; their Figure 6] which extended to 15–20 km depth. The interpretation of our longer, denser profile of higher bandwidth argues for a modern subduction and arc-related cause of the low resistivity at this latitude. If conductive shales seen in the Carbon River anticline [*Stanley et al*., 1996] are contributing to the resistivity section, they seem most likely to lie in the shallowest pod-like conductor above the paired conductor convergence. As tested with supporting information Figures S10 and S11, continuity of conductivity from near the plate interface to the upper crust appears required by the data suggesting magmatic-hydrothermal processes over a wide range of depths. We cannot comment on the full causes of the main SWCC farther south and its resolution must await further study.

The steep paired conductor discussed above correlates spatially with the Western Rainier Zone (WRZ) of seismicity, reflecting predominantly dextral strike-slip deformation [*Stanley et al*., 1996] (Figure 2). Stanley et al.'s nearest MT profile H-H' passes south of ours but it also shows a double conductor in a similar location. The WRZ is positioned within the narrow resistor separating the two conductors of *Stanley et al*. [1996] whereas in our section the seismicity appears to lie along the margin between the resistor and the eastern of the two conductors (Figure 2; as the WRZ trends ~N15W and ends at our profile, its westernmost edge should be correlated with our structure). The latter fits a common pattern where seismicity in active regimes rarely lies completely within conductors, but typically on their margins or within neighboring resistors [*Bedrosian et al*., 2004; *Ogawa and Honkura*, 2004; *Wannamaker et al*., 2009]. The resistive zones are presumed to be competent rocks capable of supporting stress, whereas the nearby conductors may contribute fluids and

help trigger failure. A closer resolution of the relation between low resistivity and WRZ deserves additional data coverage.

The boundary between the resistive forearc mantle wedge and the steep low resistivity zone in the upper mantle occurs only 20–30 km west of Mount Rainier and is correlated with the transition to the high-temperature "nose" of subarc mantle flow [*Wada and Wang*, 2009; *Grove et al*., 2012]. Its position is in keeping with heat flow constraints both from a global perspective and for Cascadia particularly [*Wada and Wang*, 2009; *van Keken et al*., 2011]. For warm plate geotherms such as Cascadia's, breakdown temperatures for peridotitic chlorite are somewhat higher than the water-saturated solidus so water-rich melt is formed directly from chlorite breakdown near the plate interface without formation of a free fluid phase [*Grove et al*., 2012]. Extrapolated from *Ni et al*. [2011] assuming efficient melt interconnection, resistivities of 10–20 ohm-m in the steep zone below the arc are consistent with melt fractions of only 1–2 vol % for the very water-rich melts (>10 wt. %) formed near the plate interface at ~100 km depth and 800–900°C, to 2–4 vol % for melts of lesser water content (~5 wt. %) but presumably higher temperature (e.g., 1200°C) in the uppermost mantle [*Grove et al*., 2012]. The temperature experienced by ascending melt is difficult to constrain precisely, especially given that the melt pathway represented by the conductor geometry is steep and seemingly confined by thick, resistant lithosphere to the east from fossil slab imbrication [*Humphreys*, 2008]. Also, melt interconnection would be nonideal and heterogeneous including channel flow textures [*Ikemoto and Iwamori*, 2014]. Nevertheless, to us establishing existence and geometry of the flux melting zone is more significant than exact melt fraction estimates. Solid-state mineral contributions to bulk conductivity are considered low, as saturated peridotite H_2O contents should only be in the 100–150 wt ppm (0.01–0.015 wt %) range [*Ferot and Bolsan-Casanova*, 2012], which the preponderance of laboratory and model analyses at present suggests contributes negligibly to lowering mineral resistivity [*Yoshino and Katsura*, 2013].

Finally, we focus on the deeper conductive zone at the far eastern end which extends beyond 200 km depth and is well resolved in the model (see supporting information). This feature is a close 2-D representation of the 3-D conductive upwelling zone labeled BA1 by *Meqbel et al*. [2014] in their 3-D inversion of the Earthscope MT Transportable Array (TA) data of the Pacific Northwest region. The region also corresponds well with the northern shear wave low velocity zone resolved by *Gao and Shen* [2014] which they ascribed to subduction-induced convective upwelling and partial fusion to yield some of the observed hot dry melts. We concur with this interpretation, supporting the argument of *Leeman et al*. [2005] for a possible role by nonflux melting at this latitude. Water contents in saturated solid-state peridotite here ~200 km depth are estimated to be in the 300–450 wt ppm range [*Ferot and Bolsan-Casanova*, 2012], with olivine concentrations somewhat lower due to partitioning with pyroxene. However, the upper limit should be bounded near 250 ppm at such depths as higher contents would induce vapor-absent peridotite melting [*Ardia et al*., 2012]. This is consistent with interpretation by *Meqbel et al*. [2014] where fertile "damp" peridotite with a few hundred parts per million intracrystalline H_2O at average mantle adiabat temperatures begins melting and dehydration at ~200 km depth during upwelling. Solid-state water contents around 250 wt ppm (0.025 wt %) most likely would reduce bulk resistivity to 50–100 ohm-m [*Yoshino and Katsura*, 2013], whereas imaged resistivity is near 10 ohm-m and thus implies melt.

3.2. EMSLAB MT Profile, Oregon

The legacy EMSLAB line crossing the Central Cascadia segment was collected in the late 1980's [*Booker and Chave*, 1989; *Wannamaker et al*., 1989], but its high-quality data makes it worth reexamining with modern analysis methods. There are 39 WB and 15 LP responses to yield a total wave period range from 0.01 s to ~7000 s at some stations. The profile length is ~220 km and average station spacing is ~5 km. The line integrates one Earthscope MT TA station at its eastern end adding to the original profile set of *Wannamaker et al*. [1989] to provide 40 sites. Our nonlinear resistivity inversion section (see supporting information Figures S12–S14) is plotted with annotation in Figure 3.

As for the CAFE-MT line, the EMSLAB model also contains a low resistivity layer deepening under the Coast Range to a distance of ~75 km inland. We again equate this dipping conductor to the presence of fluids on the plate interface generated by low-grade dehydration reactions and perhaps pore fluid collapse in altered oceanic crust. However, the updip end of this structure differs greatly from the CAFE profile. As the distinct MT impedance phase peak implies (see supporting information), conductance instead increases steadily

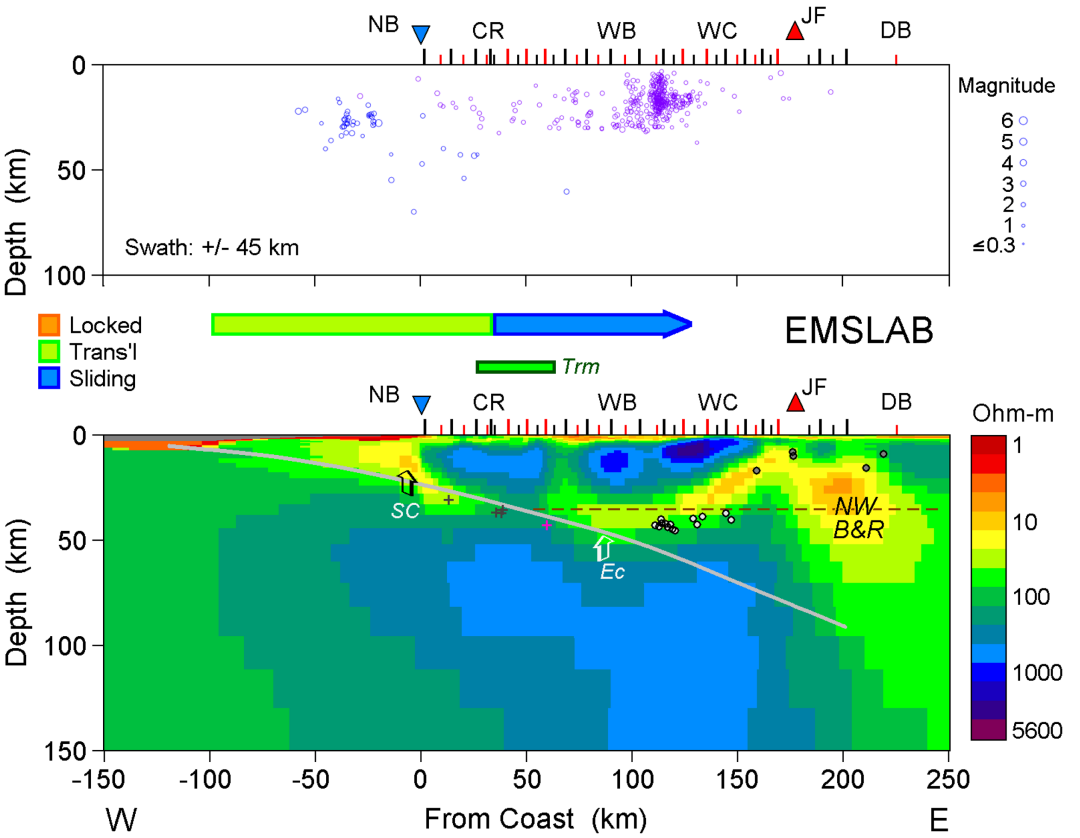

Figure 3. (bottom) Two-dimensional non-linear inversion resistivity model from MT data along the EMSLAB transect as described in supporting information. Physiographic features are offshore Newport Basin (NB), Coastal Range (CR), Willamette Basin (WB), Western Cascades (WC), Mount Jefferson (JF), and Deschutes Basin. Inverted blue triangle is coastline. LFE locations are plus symbols from *Thomas et al.* [2013] (dark gray) and *Boyarko and Brudzinski* [2010] (magenta). Eclogitization (Ec) up-arrow drawn near end of S-wave LVL coherency [*Rondenay et al.*, 2008]. Light gray-filled circles are "offset" DLP earthquakes from *Vidale et al.* [2014] with dark gray fill denoting "other." [The DLP swath is >100 km wide N-S so they are not inferred specifically below Mount Jefferson.] Abbreviations in bottom plot are subduction channel (SC), eclogitization (Ec), and northwest Basin and Range (NW B&R). Seismicity, plate surface, coupling arrow, tremor width, and Moho (35 km) as in Figure 2. (top) Definitions as in Figure 2 except seismicity swath is wider due to sparsity of events.

toward the ocean in a broad zone above the plate interface. Test calculations (supporting information Figures S15 and S16) show that a thin layer of resistive Siletz terrane rocks could be imposed at shallow levels to a distance ~40 km offshore [*Snavely*, 1987; *Trehu et al.*, 2012] and thus compress the conductor slightly, but the high conductivity could not be reduced to a thin layer 5–7 km thick at the plate interface and still fit the responses as well. Acquisition of shallow shelf marine MT data could help clarify structure in the near offshore.

The MT results in Figure 3 support previous refraction seismic interpretations [*Trehu et al.*, 2012] that sediments may be subducted beneath the Oregon continental margin. Clay mineral constituents undergoing dewatering and low-grade metamorphism may keep effective normal stresses across the plate interface relatively low, reducing transmission of stress, and thus seismicity and the horizontal width of the plate coupling zone [*Saffer and Tobin*, 2011]. However, by ~40 km inland, the conductive sediments no longer appear, leaving a deepening low resistivity layer of much reduced conductance similar to that of CAFE, explainable again by dewatering of low-grade oceanic crustal hydrous minerals. The apparent necessity of having shallow high conductivity under the near continental margin explains an earlier apparent discrepancy here between the dense passive array model of *Rondenay et al.* [2001] and the legacy forward model of *Wannamaker et al.* [1989] (see supporting information Figure S17). The latter showed that the dipping conductor was shallow under the offshore Newport Basin but the S-wave model suggested the oceanic crust was substantially deeper. The MT data mainly are sensitive to the top of the conductor rather than the bottom (depth extent) and thinness was imposed in that forward model; nevertheless, the two data types are sensing different structures under the coastal region. We believe that the possibility of significant

underthrust sediments along the central Oregon margin, together with their dewatering and low frictional properties, are consistent with models from GPS geodesy that the plate here has an obscure (if any) locked zone offshore but an unusually broad transitional zone [*Schmalzle et al*., 2014]. The MT data do not image a thick impermeable (resistive) Siletz lithology under the coastal region in the upper plate that might serve to seal high-fluid pressures.

Farther inland, the resistivity structure appears to become largely analogous to CAFE, with an increase in conductance at a depth of ~40 km and a departure from the plate interface. Correspondingly, breakdown of amphibolite facies and other hydrous minerals as described with CAFE to release free, aqueous-rich fluids as the temperature reaches ~550°C appears to be occurring, located again where the low S-wave velocity layer becomes essentially untraceable [*Rondenay*, 2001, 2008]. However, in contrast to CAFE, the conductivity increase lies arcward (east) of the FMC (Moho depth of 35 km from *Bostock* [2013]). Deepening the Moho by 5 km to be like that of CAFE does not change this result, and the depth to the 500°C isotherm does not differ by 5 km between EMSLAB and CAFE in the models of *Syracuse et al*. [2010]. Thus we consider eclogitization and fluid release by the subducted oceanic crust to be thermally controlled and not tied precisely to location of the FMC [cf., *McCrory et al*., 2014]. LFE are sparse at this latitude but we show the four identified by *Thomas et al*. [2013] using the *Royer and Bostock* [2014] technique, plus one from *Boyarko and Brudzinski* [2010] (Figure 3). These events are curious in that they extend well updip into the implied conductive sediment channel zone. We suggest that dewatering of sediments also reduces strength allowing slow slip in their domain as well. Tremor lies laterally near the inferred eclogitization or somewhat updip [*Boyarko and Brudzinski*, 2010], in some contrast with CAFE also.

Yet farther inland, and similar to CAFE, the conductive layer shallows and increases in conductance toward the arc. This is taken again to represent the continual liberation of fluids along the slab with increasing temperatures inland with a thermally controlled upper depth limit in the crust. It has been recognized for some time that most slab water and halogens do not exit the subduction system through arc volcanism [e.g., *Ito et al*., 1983; *Wannamaker et al*., 1989; and many since], and the resistivity images for CAFE and EMSLAB show that much of the fluid rises through the forearc. This is confirmed by high Br and I contents of spring flows in the forearc Willamette Basin [*Hurwitz et al*., 2005]. "Offset" deep long period (DLP) earthquakes (a form of LFE) 50–100 km frontal to the arc have been observed by *Vidale et al*. [2014] (Figure 3) near Moho levels and were suggested to reflect shallow wedge serpentine dehydration and embrittlement from imposition of Basin and Range heating. An alternate interpretation, which we prefer, is that DLP earthquakes may be associated with transit of eclogitization-derived fluids across disparate mantle-crust rheology at the Moho and into the crust, as interpreted for similar events beneath western Japan [*Aso et al*., 2013]. From resistivity, Basin and Range conditions pertain mostly from the arc eastward. Several nonoffset DLP/LFE appear toward and past Mount Jefferson arc volcano at much shallower levels (Figure 3), seemingly following the conductive layer upward. We suggest these events may represent fluids escaping across the brittle-ductile transition promoted by extensional stress, a transition which has been implicated as a permeability boundary over deep crustal low resistivity elsewhere [cf., *Wannamaker et al*., 2008].

The shallowest extent of the low resistivity also is slightly west of the arc as in Washington, as was observed previously by *Wannamaker et al*. [1989], although in part this may be the result of a data gap due to inaccessibility close to Mount Jefferson. Nevertheless, the shallow low resistivity probably now lies in the brittle domain and occupies the well-known High Cascades graben. Its normal faults extend up to 20 km west of the stratovolcano trend [*Schmidt et al*., 2008]. It corresponds closely with a similar extension of high heat flow and ^{3}He R/Ra values westward [*Van Soest et al*., 2002; *Evans et al*., 2001; *Ingebritsen and Mariner*, 2010]. Under the early Miocene western Cascades, high resistivities in the upper 10 km likely correspond to solidified intrusive rocks.

Beneath the arc and backarc areas of the EMSLAB line, the model shows the low resistivity diving eastward again but only for a relatively short depth range in contrast to the CAFE line (Figure 3). Low resistivity does not extend significantly below Moho levels with the upper mantle values being only slightly below 100 ohm-m. Such a disposition of resistivity is similar to that seen in extensional Great Basin studies [e.g., *Wannamaker et al*., 2008; *Meqbel et al*., 2014]. There, Moho level conductors indicate mafic melt underplating, possible hybridization, and hydrothermal fluid release from parental melts generation through extension in the upper mantle with temperatures near the average current mantle adiabat (ACMA, potential temperature of 1300°C). Midcrustal LFE were observed in this deep crustal zone also by *Vidale et al*. [2014]. Slab flux

melting of the upper mantle is judged to be limited for arc magmatism at the latitudes of both CAFE and EMSLAB lines [*Schmidt et al*., 2008] and does not obviously explain the pronounced difference in arc and backarc resistivity structure between the profiles.

Instead, we appeal to state of stress differences that reflect tectonic style. Regional block rotation places the northern Cascadia arc under compression whereas the central arc segment is under extension with slab rollback [*Wells and McCaffrey*, 2013]. East-west directed rifting promotes melt extraction through its coalescence into melt bands with steep dips and north-south orientations [*Kohlstedt and Holtzman*, 2009]. This alignment would not create good conductivity pathways for east-west current flow to which the TM mode data mainly used to derive the cross section are sensitive (see supporting information). A similar interpretation was made for resistivity structure of the upper mantle of the actively extensional eastern Great Basin [*Wannamaker et al*., 2008]. Because dry solid-state peridotite resistivity near the ACMA is ∼150 ohm-m [*Yoshino and Katsura*, 2013], bulk resistivities of 50–100 ohm-m are readily explained by trace amounts of residual melt. Speculatively, perhaps the more extensional stresses at this latitude compared to CAFE also promote the DLP earthquakes with fluid egress under Oregon that were not observed farther north [*Vidale et al*., 2014]. The EMSLAB profile does not extend sufficiently far eastward to capture a view of the second deep backarc upwelling BA2 imaged in the regional coverage of *Meqbel et al*. [2014], which corresponds to the second low S-wave upper mantle body of *Gao and Shen* [2014].

3.3. SWORMT MT Profile, Oregon

The 200 km long SWORMT profile in southwest Oregon was collected in 2006 and trends 60° south of east from the coast near Coos Bay to roughly 100 km inland at the California border (Figure 1). There are 45 WB and 30 LP MT stations spanning a period range from 0.01 s to ∼10,000 s with an average site spacing of 4.5 km and a total along-profile length of ∼200 km. The orientation of the SWORMT profile is distinct from our other profiles, running perpendicular to the northeast-trending boundary between the Siletz and Klamath terranes, the original target of study [*Bedrosian and Box*, 2007]. It does not reach the volcanic arc and terminates in the middle forearc region at this latitude.

Unlike the other profiles, the obliqueness of the Siletz/Klamath boundary and the profile relative to the coastline invalidates the 2-D assumption for MT data analysis. Therefore, we have inverted the SWORMT data using a nonlinear 3-D inversion incorporating an additional 30 long period EarthScope stations with 70 km spacing that fall within the domain of the 3-D model grid (Figure 1). This necessarily involves a coarser simulation grid compared to the 2-D sections and the shortest period of data analyzed is 1 s (see supporting information Figures S18–S20). A resistivity cross section along the SWORMT profile has been extracted from the 3-D inversion model and is displayed in Figure 4. We interpret this section in terms of the expected subcoastal and forearc physicochemical state.

The crust of the overlying North American plate along the northwest half of this profile differs greatly in its resistivity character from that of the older Klamath composite terrane to the southeast (Figure 4). The former shows thick, layered, low-resistivity sedimentary units corresponding to the Eocene Tyee and Umpqua Formations overlying the southernmost edge of the resistive Siletz River Volcanics. These sandstones and mudstones are faulted and folded within a series of anticlines trending perpendicular to the profile. Total thickness of these units to the northeast within the Roseburg quadrangle is ∼3 km [*Wells et al*., 2000]. At ∼75 km along the profile, a change in crustal resistivity signifies the transition to the Klamath composite terrane. The geometry of this transition is unclear, although potential-field models suggest an obduction geometry involving a southward thinning wedge of Siletz River Volcanics [*DuRoss et al*., 2002]. Southeast of the Siletz-Klamath transition, massively resistive Paleozoic and Mesozoic igneous and metamorphic formations within the Western Klamath and Hayfork arc terranes are encountered. These are in turn intruded by the resistive Cretaceous Grants Pass, Grayback, and Ashland intrusive complexes, the roots of which appear to extend to the base of the crust.

In contrast, especially with the adjacent EMSLAB profile to the north, the resistivity along plate interface depths from below the coast to ∼35 km inland (70 km along the profile) is moderately high (100s of ohm-m) (Figure 4). This implies a lack of subducted sediments or fluids being released from low metamorphic grade hydrous minerals. Test calculations (see supporting information Figures S21 and S22) where a conductive layer is inserted atop the plate from the trench to a slab depth of ∼30 km give rise to a distinct impedance phase peak not observed in the measured MT data within 30 km of the coast. This lack of

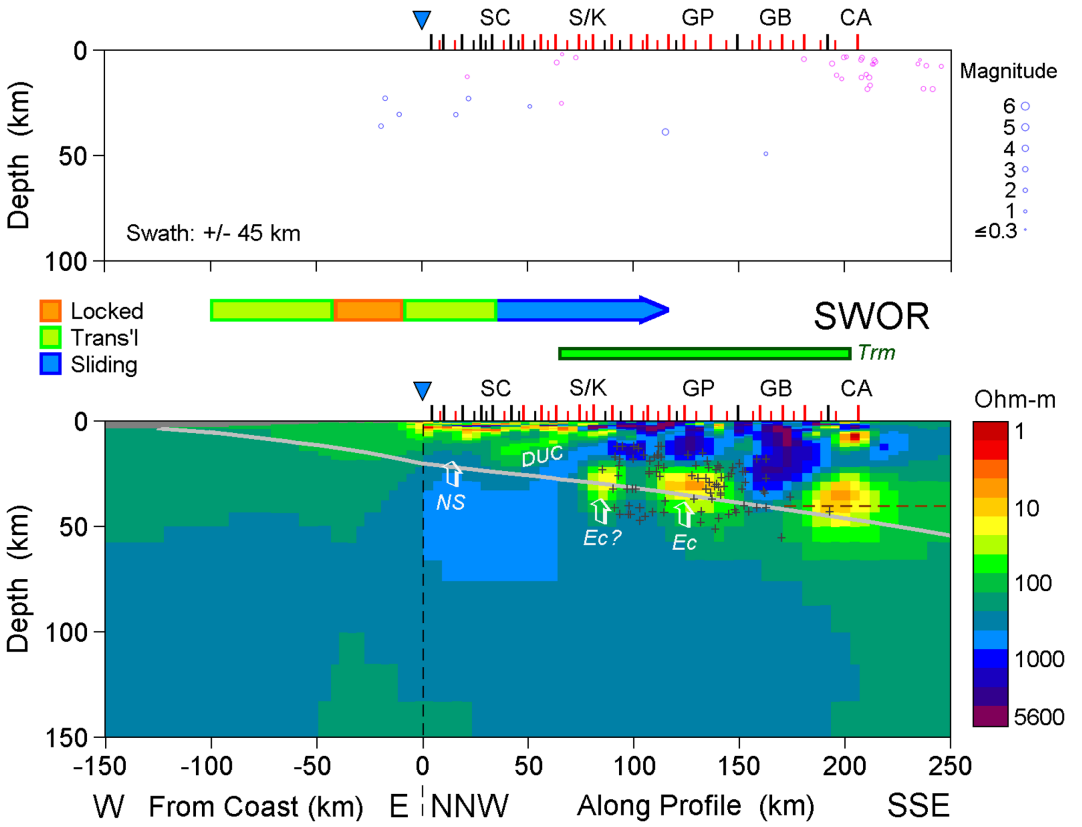

Figure 4. Section view along dense SWORMT profile extracted from overall 3-D nonlinear inversion resistivity model as described in supporting information. Vertical-dashed line marks bend in section where seaward panel is east-west while landward panel is northwest-southeast. Physiographic features are South Coastal Basin (SC), Siletz/Klamath transition (S/K), Grants Pass pluton (GP), Grayback pluton (GB), and California border (CA). Inverted blue triangle is coastline. LFE locations are dark gray plus symbols in a ±10 km swath from *Boyarko and Brudzinski* [2010]. Abbreviations in bottom plot include no sediments (NS), deep upper plate conductor (DUC), and eclogitization (Ec). Seismicity, plate surface, coupling arrow, and tremor width as in Figure 2. Moho (40 km) extrapolated from *Liu et al.* [2012]. Given the profile orientation, features are substantially elongate left to right relative to an east-west, geotectonic cross-strike assumption. To obtain cross-strike distances, the along-profile distances plotted may be divided almost exactly by two. (top) Definitions as in Figure 2 except seismicity swath is wider due to sparsity of events.

conductance is more akin to the CAFE line under the Washington coast. The apparent absence of conductive fluids and sediments within this region is somewhat unexpected given the lack of seismicity; similar resistivity structure along the CAFE and Klamath-Modoc (next) lines is accompanied by moderate and extensive seismicity, respectively. Furthermore, sediment balance analysis by *McNeill et al.* [2013] suggests that for the southern Oregon margin either substantial sediment is subducted or removed via strike-slip motion. Nevertheless, the high plate interface resistivity correlates with the inference of elevated plate coupling offshore by *Schmalzle et al.* [2014] projecting onto our transect from ~15 to 100 km in along-profile distance.

At distances of 30–70 km along the profile, a modest low resistivity zone exists in the 7–15 km depth range shallowing to the southeast (DUC feature of Figure 4). It produces a small impedance phase peak in the MT responses measured above it (see supporting information) but this peak occurs at periods too short to correspond to a conductor along the plate interface as seen in the EMSLAB and CAFE measurements. Although conceivably this structure could result from fluids risen from the slab below, it is curious that it would have such a limited lateral extent and that such a feature is not observed on any of the other profiles. Speculatively, it could be older and associated with collision of the Siletz terrane upon the Klamath, but we have no further constraints upon its cause. Farther inland, resistivities are high again from the overriding lower crust through the plate interface. It is remarkable that no interface conductor at all is resolved, again unlike the case for EMSLAB and CAFE; perhaps there is a particular stress regime associated with the Siletz-Klamath transition that inhibits retention of fluids in this area.

More pronounced increases in conductivity are seen starting at distances of ~80 km along the profile (Figure 4). There is a clustering into three concentrations starting just southeast of the Siletz-Klamath transition. This is again attributed to breakdown of amphibolite facies and other hydrous minerals. The discrete nature of these compact conductors contrasts with the corresponding structures below the northerly profiles. We do not interpret them as concentrated zones of mineral dehydration per se. Instead we suggest that the highly resistive, Cretaceous intrusive bodies and their lower crustal roots in the Klamath terranes are relatively impenetrable and strongly influence the pathways and residence locations of fluids exsolved upward from the slab. We believe such behavior also is seen under the Klamath-Modoc and ABCS transects discussed below. Onset of LFE [*Boyarko and Brudzinski*, 2010], although less accurately constrained in depth compared to the northerly profiles, again corresponds to the beginning of low-resistivity eclogitization (Figure 4). In terms of ETS recurrence intervals, the SWORMT line lies in the transition from the Siletzia zone with a low recurrence rate to the Klamath zone with a high rate [*Brudzinski and Allen*, 2007]. Note that the steeply south orientation of the profile elongates the features in this section view left to right by a factor of two relative to an east-west, cross-strike assumption, and irregularities can be expected along the leading edge of the eclogitization front.

3.4. Klamath-Modoc MT Profile, California

The profile across northern California contains new MT data gathered from 2009 through 2013, and not previously analyzed. It passes over the Gorda segment of the Juan de Fuca plate and crosses the Southern Cascadia arc segment just north of the LVC. There are 95 WB and 19 LP responses with a total period range from 0.005 s to as long as ~17,000 s. The profile length is nearly 400 km and average station spacing is ~4 km. The 2-D nonlinear resistivity inversion model, analysis of which is described with supporting information Figures S23–S27, is shown in Figure 5.

The California section shows some similarities but also significant differences from profiles discussed previously. Similar to SWORMT, but in contrast to CAFE and EMSLAB, there is no apparent low resistivity layer dipping inland from near the coast to distances of ~75 km. From 20 to 100 km inland, the plate interface as modeled by *McCrory et al*. [2012] is overlain by a low-resistivity crust of substantial thickness, which corresponds to previously underthrust Franciscan Formation. This body also is characterized by low V_S [*Liu et al*., 2012]. It is certainly possible that a weak low-resistivity layer along the Juan de Fuca plate interface would be masked by the Franciscan especially if it is in immediate basal contact. A short distance east of South Mountain Ridge, a thin outcropping resistive unit is taken to represent overthrust Klamath terrane rocks of higher metamorphic grade [*McLaughlin et al*., 2000].

However, the resistivity directly under the coastline and vicinity is strikingly high, more so even than under the CAFE and SWORMT profiles. Rocks of several hundred ohm-meter exist well above the plate interface to within several kilometers of the surface (Figure 5). Very little in the way of conductivity is permitted in this part of the model by the data (see supporting information Figures S28–S30). High resistivity suggests high levels of plate interface coupling at least locally, certainly compared to Oregon or even northern Washington. It points to the possibility of stress buildup associated with the north-south compression across the Mendocino triple junction, consistent with high earthquake activity in the region [*McCrory et al*., 2012] (Figure 5). The very high resistivities above the plate support McCrory's speculation based on abundant shallow seismicity that a fragment of the Gorda plate may have detached under the coastline. Possibly analogous, relict intrasubduction serpentinites are observed to the south in the Franciscan Formation [*McLaughlin et al*., 1982; *Prohoroff et al*., 2012].

The MT results provide some interesting details below the coastal Eel River Basin about the southern Juan de Fuca plate subduction (Figure 6). High resistivities of the shallow plate are overlain by moderately folded and thrust-deformed conductive sedimentary units of the basin [*McLaughlin et al*., 2000]. The conductive layer at ~2 km depth that is quasi horizontal for the 4–5 coastal sites and then rises steeply to the surface near site 6 coincides with the Late Cretaceous, shaly Yager Formation. The upper more resistive unit confined within the synclinal Yager corresponds to depositionally overlapped, semiconsolidated clastic rocks of the Wildcat Group of mid-Miocene to Pleistocene age. This described geometry corresponds precisely with the structural cross section drawn through here by *McLaughlin et al*. [2000]. An eastward tapering, horizontal conductor in the upper few hundred meters under the three westernmost sites we hypothesize to be a seawater incursion within the Wildcat. The observed sounding at site 2 is shown in supporting information

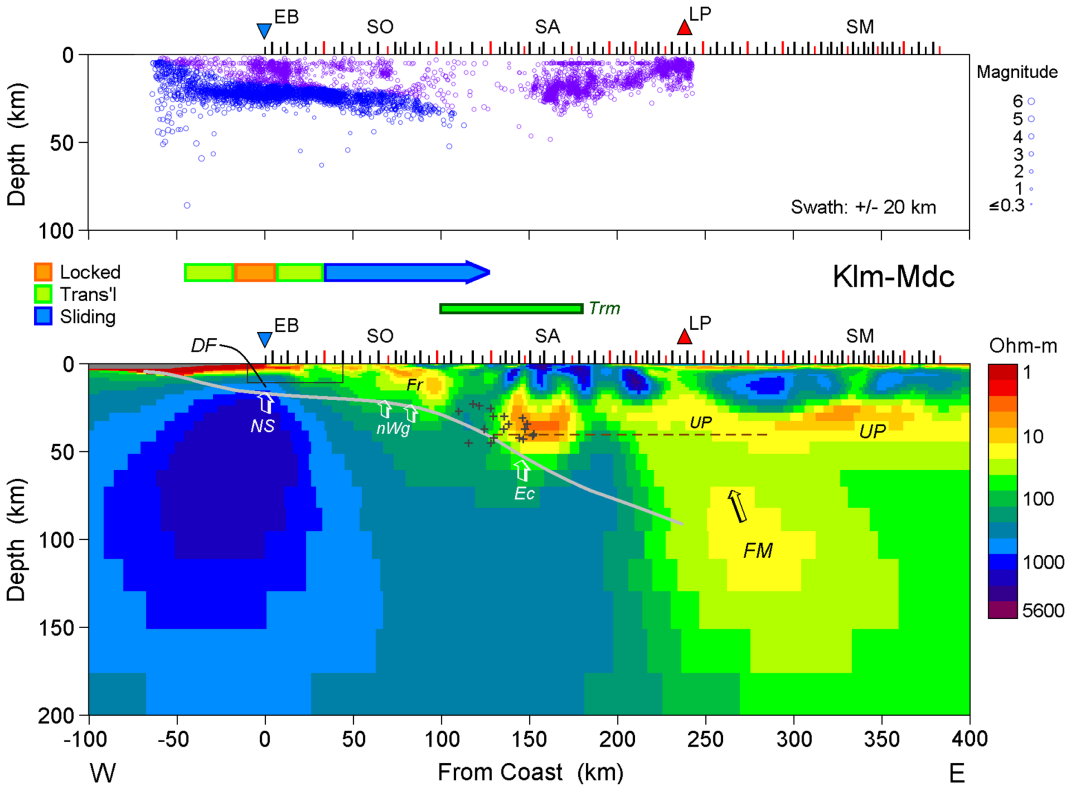

Figure 5. (bottom) Two-dimensional nonlinear inversion resistivity model from MT data along the Klamath-Modoc transect as described in the supporting information. Physiographic features are Eel River Basin (EB), South Mountain ridge (SO), Sacramento River (SA), Lassen Peak (LP), and Shinn Mountain (supporting information). Inverted blue triangle is coastline. LFE locations are dark gray plus symbols in a ±35 km swath from *Boyarko and Brudzinski* [2010]. Abbreviations in bottom plot include no sediments (NS), detached Gorda plate fragment (DF), no mantle wedge (nWg), underthrust Franciscan Formation (Fr), eclogitization (Ec), flux melting (FM), and underplating (UP). Eclogitization (Ec) up-arrow drawn near beginning of Moho hole (lack of seismic contrast) of *Liu et al.* [2012]. Seismicity, plate surface, coupling arrow, and tremor width as in Figure 2. Moho (40 km) from *Liu et al.* [2012]. Thin rectangle under Eel River Basin denotes area of Figure 6. (top) Definitions as in Figure 2.

Figure S31 and exhibits two apparent resistivity minima denoting the incursion and the Yager Formation rocks. The subvertical to steeply east-dipping, moderately resistive material under site 7 and eastward coincides with Central Belt melange of the Franciscan Formation thrust against Yager Formation [*McLaughlin et al*., 2000]. Finally, although precise interface picking is at odds with the concept of smooth tomographic-style MT inversion, rising resistivities at depth suggest Gorda Plate material is encountered by ~7 km (Figure 6). This would be the detached fragment, with the subduction interface at a depth of 15–20 km [*McCrory et al*., 2012].

The shallow dip of the southern Juan de Fuca plate continues inland to a distance just over 100 km, whereupon the plate dives steeply (Figure 5). At ~150 km from the coast above the plate, below the Sacramento River, a rather compact low resistivity body appears in the 15–50 km depth range. Although thermal models of this plate configuration are not published, this feature appears likely to be a zone of sudden fluidization from eclogitization of the quickly descending plate. Slow slip earthquake waveforms (LFE) were identified visually by *Boyarko and Brudzinski* [2010] and location testing suggested depth uncertainties up to 15 km with epicentral locations perhaps one-third of that. Nevertheless the epicenters are estimated to lie near and just updip of our conductor (Figure 5), comparable to the CAFE and SWORMT profiles where negligible sediments also are inferred to be subducted. Moho estimates are variable in this region [*Liu et al*., 2012] with an average near 40 km, and so the conductor lies arcward of the FMC. The conductor is approximately coincident with a subtle low V_S zone in the 25–35 km depth range identified as possible fluids from eclogitization by *Liu et al*. [2012], who also note reduction of Moho contrast as seen in the S-wave surveying over the EMSLAB and CAFE lines. It corresponds as well to a low V_P body imaged by *Thurber et al*. [2009] that they did not specifically discuss.

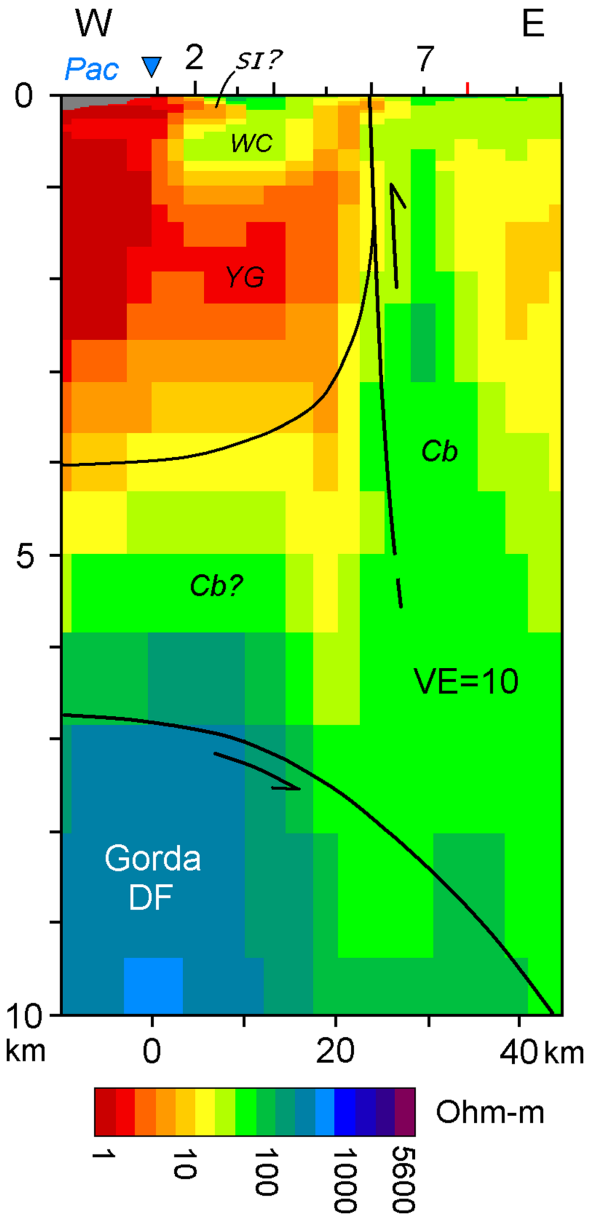

Figure 6. Detailed close-up of resistivity structure below the Eel River Basin, coastal northern California, from our MT transect and inversion. Pacific Ocean (Pac) seawater in gray. Geological units are the Wildcat Group (WC) and Yager Formation (YG) and Central Belt (Cb) of Franciscan Formation. Structure in part after *McLaughlin et al.* [2000]. Shallow near-coastal conductor is speculated to be seawater incursion (SI?). Note that high vertical exaggeration distorts thickness of horizontal segments such as that of the buried Yager Fm relative to its steep eastern limb. Gorda Plate detached fragment (DF) equated with resistivities exceeding ~300 ohm-m.

Perhaps because of the suddenness of the fluid release just described, there is not a continuous layer of interpreted slab-released fluid shallowing toward the arc on this profile. There also are several resistive bodies imaged in the middle crust, probably associated with various plutons of the eastern Klamath terrane [*Allen and Barnes*, 2006], which may be adequately competent to impede or divert upwelling fluids as under SWORMT. As the LVC is approached, there is a modest, quasi tabular conductor near Moho levels which possibly represents magmatic underplating from deeper sources. A subtle lower resistivity body in the upper middle crust (<10 km depth) may be a zone of broader fluid accumulation and extensive normal faulting in the corridor between Lassen and Crater Peaks to the north [*Clynne and Muffler*, 2010]. It is offset somewhat west of Lassen Peak but, since our profile lies to the north by 15–20 km and fault strikes are somewhat west of north, much of this may be projection. With the dense sampling through here, we were able to resolve a low-resistivity axis extending through the brittle crustal domain in contrast to *Park and Ostos* [2013], whose WB station density was 5–7 times less than ours.

Deeper under the LVC, the model contains a large confined conductor in the 70–120 km depth range (Figure 5). Test inversion in the supporting information that assumed a N025W geoelectric strike as used by *Park and Ostos* [2013] placed a similar body of somewhat lower resistivity in the 50–100 km range. This is acceptable agreement given the ability of MT data to resolve the lower limits of bodies. LVC and neighboring Mount Shasta exhibit the highest degrees of slab input, flux melting, and silica enrichment of volcanic products in the Cascades chain [*Schmidt et al.*, 2008; *Grove et al.*, 2012]. The low-resistivity volume lies just above the plate interface, consistent with the expected depth range of slab flux melting (FM). Similar to discussion with CAFE, melt fractions of only 1–2 vol % should suffice to explain the anomaly. The conductor domain corresponds well with the low V_S body in the 50–80 km depth resolved by *Liu et al.* [2012] and interpreted to be due to H_2O-induced melting. Stresses from LVC through the southern Modoc Plateau to the Great Basin area transition from strike-slip/slightly transtensional to predominantly extensional [*McCaffrey et al.*, 2013]. Thus the low-resistivity variations near the arc on the southerly line are not restricted to Moho levels as was the case for the EMSLAB backarc, where extensional melt banding and egress were interpreted. Nevertheless,

local stress changes or extension can tap diverse, primitive upper mantle magmas that are little modified to eruption [*Muffler et al*., 2011].

Toward the eastern end of the profile in the 290–370 km lateral range, a tabular low resistivity region occurs near Moho and lower crustal depths (Figure 5). This feature underlies the southernmost extent of the late Miocene and younger trend of primitive basaltic lavas of the southern Modoc Plateau, interpreted to form in the shallowest upper mantle (41–51 km nominally) from nearly anhydrous decompression [*Till et al*., 2013]. The decompression in turn was driven by subduction-induced corner flow and upwelling in the mantle wedge. This is a somewhat more extensional regime than that of the arc volcanoes to the west, and the resistivity structure now more resembles that of the Great Basin [*Wannamaker et al*., 2008] where underplating structure dominates and there is little upper mantle melt with long-range E-W interconnection [*Kohlstedt and Holtzman*, 2009]. Nevertheless, some primitive melts do pass completely through to the surface [*Till et al*., 2013]. The third deep upper mantle upwelling zone inferred in the Transportable Array S-wave imaging again lies off the east end of our profile, in western Nevada [*Gao and Shen*, 2014]. Curiously, that upwelling is not coincident with low resistivity upwelling BA3 of *Meqbel et al*. [2014], which lies south of the eastern end of our line.

3.5. Comparison with Prior ABCS MT Profile

Thirty-three MT soundings were collected in 2003 on a 460 km long profile across Vancouver Island and southwestern B.C., and referred to as the Alberta-British Columbia South (ABCS) transect [*Soyer and Unsworth*, 2006; *Rippe et al*., 2013], to which we added one Earthscope MT TA site (Figure 1). These are long period (LP) responses only (see supporting information) with a signal period range of 4.3–10,240 s and thus are sensitive mainly to structure from the middle crust through the upper mantle. Given the reduced bandwidth and coarser spacing (13.5 km average), structural resolution will be decreased compared to our other profiles. Moreover, the profile effectively starts 40 km farther from the trench than does CAFE, and so relating resistivity below Vancouver Island to plate locking is difficult. Nevertheless, worthwhile correlations can be made with the other profiles and subduction processes along the length of Cascadia, and it is valuable to compare resistivity models using a common inversion approach. Our 2-D nonlinear resistivity inversion section for ABCS is plotted with annotation in Figure 7 and MT data response pseudosections are in supporting information Figure S32.

Having only seven sites on Vancouver Island, two of which exhibit 3-D complexity (see supporting information), limits inferences there. Resistivity values offshore remain close to the starting model value reflecting lack of resolution, while under the western part of the island there is a weak resistivity minimum at the plate interface similar to that of CAFE [*McCrory et al*., 2012] and is based mainly on the MT responses of sites 2 through 4 from the coast (see supporting information Figure S32). A similar minimum is seen in the inversion of the more coarsely spaced ABCN profile of *Rippe et al*. [2013] farther north across Vancouver Island incorporating the data of *Kurtz et al*. [1986]. Under the eastern part of the island, a large low-resistivity body labeled E lies above the plate boundary and is equivalent to one imaged by *Soyer and Unsworth* [2006] and *Rippe et al*. [2013]. This conductor obscures the imaging of resistivity directly associated with interface processes in this area, and a lack of sampling across the Georgia Strait exacerbates the problem.

The E-conductor name is derived from the observation of a package of high seismic reflectivity (E-horizon) below Vancouver Island in the 20–35 km depth range, originally believed to lie significantly above the plate interface [*Kurtz et al*., 1986]. The reflectivity has been equated to a seismic low P-wave velocity zone assigned to lithology within the upper plate (part of Wrangellia), with the Juan de Fuca plate up to 15 km deeper [*Ramachandran et al*., 2006]. This gave rise to the concept of fluids rising from the slab either from pore collapse or mineral dehydration, and being trapped at higher levels through retrogression and mineral precipitation [*Hyndman*, 1988; *Kurtz et al*., 1990]. On the other hand, the S-wave LVL imaged for Vancouver Island was argued to lie close to the E-horizon and be the oceanic crust itself [*Bostock*, 2013]. The plate interface model of *McCrory et al*. [2012] is more closely referenced to the transition to mantle velocities in the P-wave model and thus lies up to 10 km deeper than that from the S-wave LVL. In some studies, the LVL is suggested to be a melt, fluid, or sediment layer overlying the subducted oceanic crust [e.g., *Wada and Wang*, 2009; *Calvert et al*., 2011]. The variability in seismic interpretation is unresolved at present.

LFE locations estimated by *Royer and Bostock* [2014] are plotted in Figure 7 and, as they noted, lie between the plate interface models of *McCrory et al*. [2012] and *Bostock* [2013]. This is unlike the closer

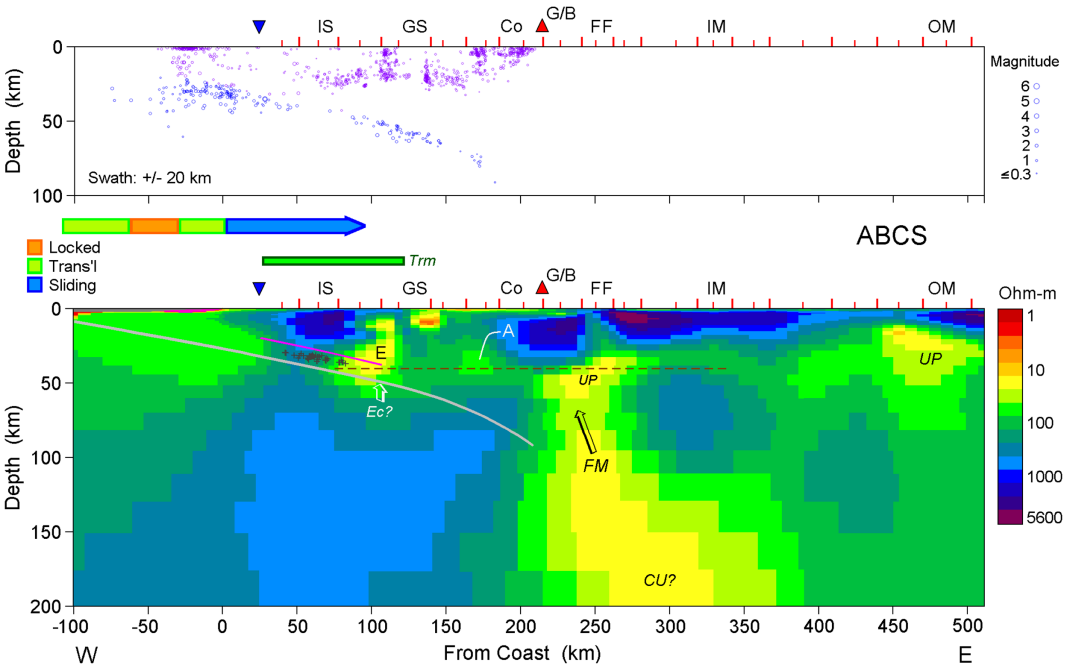

Figure 7. (bottom) Two-dimensional nonlinear inversion resistivity model from MT data along the ABCS transect as described in supporting information. Physiographic features are Insular subterrane of Wrangellia on Vancouver Island (IS), Georgia Strait (GS), Coastal Belt (Co), Mount Garibaldi/Mount Baker volcanic arc axis (G/B), Fraser fault zone (FF), Intermontane Belt (IM), and Omineca Belt (OM). Subducted plate interface follows *McCrory et al.* [2012]. LFE locations (dark gray plus) are in a ±20 km swath from *Royer and Bostock* [2014] and magenta band is top of S-wave LVL [*Bostock*, 2013]. Abbreviations in bottom plot include E-conductor (E), A-conductor (A), magmatic underplating (UP), flux melting (FM), and possible backarc upwelling (CU?). Eclogitization (Ec?) up-arrow drawn near end of S-wave LVL coherency [*Bostock*, 2013]. Seismicity, coupling arrow, tremor width and Moho (35 km) as in Figure 2. (top) Definitions as in Figure 2.

correspondence between McCrory and coworkers and the LFE on the CAFE and EMSLAB lines, although the McCrory and coworkers model for EMSLAB is based more upon active source profiling and S-wave tomography than the sparse seismicity. In the context of the other MT profiles, such a sudden occurrence of conductivity due to subducted plate eclogitization is unexpected given the gentle and steady descent of the plate. The position of the E-conductor (Figure 7) also coincides with a major sinistral transpression zone as the Insular subterrane of Wrangellia docked with the B.C. mainland [*Monger et al.*, 1994]. Thus, we cannot overrule a contribution of downthrust trapped metasediments to the low-resistivity E-conductor. That accreted sediments as old as Eocene under the Olympic Mountains are still of low resistivity [*Aprea et al.*, 1998] illustrates the possible persistence of sedimentary body effects unless dehydrated by high-grade metamorphism. The previously underthrust Franciscan Formation rocks of the Klamath-Modoc profile represent a similar situation.

The situation simplifies east of Georgia Strait (Figure 7). Resistive crustal rocks of the Coastal Belt plutonic complex permit resolution of a quasi horizontal, Moho-level conductor extending to the volcanic arc axis that equates to the A-conductor of *Soyer and Unsworth* [2006] and the B-conductor of *Rippe et al.* [2013]. The conductor is analogous to the deep crustal layer seen under the near forearc of CAFE interpreted as fluids that have risen to the deep crust from progressive slab dehydration. Under ABCS, we do not see this layer shallowing toward the arc as with CAFE, which we interpret to reflect impermeable batholithic Coastal Belt rocks. This geometry is more similar to the Klamath-Modoc line. In the upper mantle below the arc, a low-resistivity zone extending to the bottom of the displayed section at 200 km is considered analogous to the interpreted flux melting structure imaged with the CAFE profile and the asthenospheric conductor of *Soyer and Unsworth* [2006] and *Rippe et al.* [2013]. It is possible that its deeper reaches reflect some convective upwelling such as interpreted under CAFE. There is a corresponding conductive structure at middle upper mantle depths under ABCS appearing, albeit more faintly, in the 3-D model of *Meqbel et al.* [2014]. However, this lies just outside the Earthscope MT TA array to its north and is not considered well resolved.

A confined Moho-level conductor below and east of the arc axis is consistent with limited magmatic underplating similar to CAFE, and fluids exsolved therefrom may be penetrating the Fraser River fault zone.

Subd Domain	Sub-Coastal	Distal Forearc	Near Forearc	Arc	Backarc
Arc Segment					
Northern (ABCS)	-Moderately High Resistivity (ρ)? -Sediments Unclear -Modest Seismicity -Strong Coupling	-Accretionary Material Obscures -Conductor near Plate Interface -Transitional Coupling	-Progressive Low-ρ Eclogitization -Exsolved Fluids Along Moho -LFE near Onset of Eclogitization	- Low-ρ Flux Melting Structure Directly Under Arc -Possible Deeper Low-ρ Upwelling (Non-Flux) Comp.	-Weak Moho Conductor below Near Backarc - Moderately high-ρ, Weakly Extensional Upper Mantle
Columbia (CAFE-MT)	-Moderately High Resistivity (ρ) -No Sediments -Modest Seismicity -Strong Coupling	-Dipping Plate Conductor -Transitional Coupling	-Progressive Low-ρ Eclogitization -Exsolved Fluids Rise Toward Arc -LFE at Onset of Eclogitization	- Low-ρ Flux Melting Structure Directly Under Arc -Possible Deeper Low-ρ Upwelling (Non-Flux) Comp.	-Compressional High-ρ Lithosphere to Upmost Mantle -Deep Convective Asthenospheric Low-ρ Upwelling
North Central (EMSLAB)	-Low Resistivity -Subd Sediments -Scarce Seismicity -Weak Coupling	-Dipping Plate Conductor -Transitional Coupling	-Progressive Low-ρ Eclogitization -Exsolved Fluids Rise Toward Arc -Widespread LFE's Along Fluid Layer	-Subarc Resistivity Control by Extensional Textures -Flux Melting Component Texturally Obscured	- Low-ρ Melt Underplating -Moderately high-ρ, Extensional Upper Mantle
South Central (Forearc) (SWORMT)	-Moderately High Resistivity (ρ) -No Sediments -Scarce Seismicity -Moderate Coupling	-No Dipping Plate Conductor -Transitional Coupling	-Progressive Low-ρ Eclogitization -Weak Continuity of Fluids Toward Arc -LFE at Onset of Eclogitization	N/A	N/A
Southern (Klm/Mdc)	-High Resistivity -No Sediments -High Seismicity -Strong Coupling/ Detachment	-No Dipping Plate Conductor -Transitional Coupling	-Sudden Low-ρ Eclogitization -Weak Continuity of Fluids Toward Arc -LFE at Onset of Eclogitization	- Low-ρ Flux Melting Source Zone -Minor Moho-level Low-ρ Underplating	- Low-ρ Melt Underplating -Moderately high-ρ, Extensional Upper Mantle

Figure 8. Tabular summary of resistivity geophysical properties with physicochemical implications across subduction subdomains and along volcanic arc segments of the Cascadia subduction system.

A subtle low-resistivity layer at Moho levels continues eastward under the Intermontane Belt, and then amplifies and moves to shallower levels below the Omineca belt (Figure 6). High heat flow and isostatically compensated, thinned crust imply mantle heat convection in these backarc terranes [*Hyndman et al.*, 2005; *Soyer and Unsworth*, 2006; *Hyndman and Currie*, 2011; *Rippe et al.*, 2013], with adiabatic upwelling and fusion delivering mafic melts to the lower crust that cool and release conductive fluids upward [cf., *Wannamaker et al.*, 2008]. The particularly strong expression under the Omineca belt correlates with early to middle Tertiary crustal extension and persists across its entire width [*Ledo and Jones*, 2001; *Rippe et al.*, 2013].

4. Synthesis and Conclusions

The along-strike variations in the Cascadia subduction system provide an opportunity to more fully understand the variety of processes and physical states operating in subduction zones generally. We summarize similarities and differences along the system in Figure 8. Pronounced changes in the electrical resistivity correlate with the degree of geodetically inferred plate locking and width of transitional zone, where sections of greater locking correspond with higher resistivity. Cause versus effect is ambiguous here; it is unclear whether lack of fluids induces the locking or whether variation in stress from other factors controls the fluid distribution. Channeled sediments are suggested to help explain low resistivity and the weaker locking of the north-central Oregon subduction margin; perhaps Siletz terrane composition has a mechanical influence that promotes sediment underthrusting. Subducted sediments with low-temperature fluid release also have been interpreted to cause weak plate coupling and low resistivity along and above the plate interface of the northern Hikurangi margin in New Zealand, whereas strong coupling and high resistivity are characteristic of its southern margin [*Heise et al.*, 2013]. The relation to forearc seismicity is less clear, however, in

that southern Oregon exhibits the lowest seismicity of Cascadia while plate coupling appears elevated compared to northern Oregon.

Some aspects of Cascadia resistivity structure exhibit substantial along-margin continuity. Both the Oregon (EMSLAB) and Washington (CAFE) transects show a deepening conductor near the subduction interface that probably represents fluids originally trapped or newly generated by dehydration. Possibly the presence or absence of the low resistivity layer along the margin reflects variation in degree of silica sealing and fluid entrapment [e.g., *Audet and Burgmann*, 2014], but this aspect of the resistivity does not appear to correlate with ETS recurrence interval. An increase in conductivity along all profiles as the mantle wedge is approached suggests that a sudden increase in dehydration occurs where temperatures reach 500–550°C, in keeping with eclogitization implied from petrology [*van Keken et al*., 2011]. On the other hand, the commencement of low resistivity does not bear a precise correspondence to the forearc mantle corner; on the CAFE and Klamath-Modoc lines it appears arcward of the FMC whereas under EMSLAB and SWORMT it appears trenchward. Although a progression to stable sliding with increased temperature is well-founded, and temperature increases can release fluids through reaction, the relatively direct evidence from conductivity where the apparent end of transitional plate locking occurs implicates fluids more directly in the final strength gradation to stable sliding.

The significance of the gap between the geodetically defined edge of plate coupling and the Cascadia tremor band [*McCrory et al*., 2014] is obscure. However, the presence of a deepening conductor here (albeit subdued) below CAFE and EMSLAB plus high fluid pressures inferred from seismic velocities [*Audet et al*., 2010] suggest that this zone also is weak given that water content of just a few tenths volume percent can make the rock strength extremely low through reduction of effective normal stress plus the promotion of diffusion creep [*Tullis et al*., 1996; *Sibson*, 2007]. LFE are clustered in both northern and southern Cascadia near where eclogitization commences, but are more diffuse in the central section along possible subducted sediment. Numerous LFE have been observed at much shallower depth and lower temperatures below the northern Hikurangi and northern Japanese margins, and are interpreted to be associated in part with subducted sediment dewatering [*Wallace et al*., 2012; *Heise et al*., 2013; *Ito et al*., 2013]. In locked southern Hikurangi, the LFE are from 30 to 50 km depth, as in the more coupled Cascadia sections.

The CAFE and EMSLAB Cascadia segments show liberated fluids rising into the crust toward the arc, presumably altering the upper mantle wedge along the way and in turn being transformed by chemical exchange. Details of fluid pathways in the crust depend upon rheology, however, and coherent plutonic roots impede or deflect fluid transit toward the surface under the SWORMT, Klamath-Modoc and southern B.C. profiles. A detailed MT transect from the Pacific coast across the Trans-Mexican Volcanic Belt into its backarc by *Jodicke et al*. [2006] revealed a lower crustal conductor developing above the subducting young, shallow-dipping Cocos plate shortly after it enters the mantle wedge. The conductor is coincident with clustering of NVT above, and LFE along, the subduction slip plane of that area [*Husker et al*., 2012; *Frank et al*., 2013], consistent with Cascadia. Arima-type hotspring fluids, interpreted as subduction-derived, overlie low resistivity, and high V_P/V_S anomalies plus an LFE swarm near the FMC of the southwestern Japan forearc [*Umeda et al*., 2006; *Kato et al*., 2014; *Kusuda et al*., 2014]. In those profiles and ours, fluid release from eclogitization appears to start ~100 km from the arc implying thermal control. A global compilation of forearc conductors by *Worzewski et al*. [2011] showed a roughly consistent distance between those conductors and the arc, even for diverse geometries and thermal regimes including Chile and Japan (the precise distance they chose reflects location center more than leading edge). *Peacock* [2009] argued that fluidization could occur at similar depths in slabs having differing thermal regimes, with the varying thermal trajectories crossing distinct hydrous mineral breakdown boundaries. On the other hand, a coherent S-wave LVL can be traced to depths near 100 km along the older (formed 40–50 Ma at trench) Pacific plate beneath Alaska and central Chile [*Rondenay et al*., 2008; *Bostock*, 2013] suggesting limited fluidization prior to that.

Large, along-margin variations in arc and backarc structure related to melting processes have been revealed in the electrical resistivity models as well. Resistivity structure suggests that the transition from cold forearc mantle wedge to hot subarc wedge occurs nearly directly under the arc, or at most 20–30 km trenchward. In the north, structure compatible with flux melting is resolved even though the degree of fluxing is judged to be limited. However, decompression melting from deep subduction-induced upwelling also may contribute to the melt supply. The hydration of such deep volumes might not be entirely from the current subduction regime; in concept some could be related to the vanished Farallon plate. Resistivity structure here

resembles that in the central Andes of Bolivia [*Brasse and Eydam*, 2008] where we suggest that their very large backarc conductor could be explained by similar deep upwelling and decompression. Direct subarc conductivity is relatively subdued beneath the central Andes, perhaps a result of fluxing fluids being carried much deeper. On the other hand, despite a cold subducted plate, a strong Moho-level or lower crustal conductor was resolved under the northern Honshu Japan arc by *Kanda and Ogawa* [2014] although depth resolution admittedly was limited to ~80 km in that array. Globally, both forearc and backarc anomalies in resistivity and seismic attenuation may correlate in amplitude [*Pommier*, 2014].

Farther south in central Cascadia, comparison of the EMSLAB arc and backarc with CAFE indicates that state of stress and deformation regime (extension versus compression) may be important factors in addition to pressure-temperature composition controls for determining the nature of the electrical geophysical structure. Similar to the EMSLAB line and perhaps the southern Modoc Plateau, the backarc area of the Trans-Mexican Volcanic Belt may be undergoing extension particularly at depth. Alkaline basaltic and bimodal volcanism has occurred there through Pliocene time and a broad Moho-level conductive zone is observed [*Jodicke et al*., 2006]. In southern Cascadia, supraslab resistivity confirms that subduction flux melting and other slab inputs are substantial. Current deformation and geophysical structure at the Gorda coastal area, however, imply that subduction inputs may be dynamic and time-varying, and perhaps not entirely representative of past inputs now affecting the arc.

Acknowledgements

Phil Wannamaker and Virginie Maris gratefully acknowledge funding by the U.S. National Science Foundation under grants EAR08–43725 and EAR08–38043 through the Earthscope and Geophysics programs. The 2D inversion capability received development support under U.S. Department of Energy contract DE-PS36-04GO94001. Rob Evans was supported through Earthscope grant EAR08–44041 and Shane McGary through a National Defense Science and Engineering Graduate (NDSEG) fellowship. Fieldwork in Canada was made possible by an NSERC Discovery Grant and a Canadian Foundation for Innovation award to Martyn Unsworth. The long period instruments were borrowed from the University of Washington (John Booker, P.I.) through the NSF-supported EMSOC national MT pool. Steve Park generously shared the five NIMS responses he measured across Lassen National Forest. We thank Mike Baker, Joe Borman, Heather Haley, Teatha van Schooten, and Adam Vicinus for field assistance in the long period CAFE and Klamath-Modoc collection. Quantec Geoscience Inc acquired the wideband MT data of the CAFE line and the great majority of the Klamath-Modoc line. Mike Brudzinski, Alexandra Royer, and Amanda Thomas kindly provided location files for the LFE events along Cascadia. Pat McCrory shared a link to the seismicity data from her 2012 paper and provided many useful comments. Content and presentation benefited substantially from the remarks of two anonymous reviewers. We are grateful to the U.S. Bureau of Land Management, U.S. Forest Service, Latour State Forest, the Beaty, Green Diamond, Hancock, Humboldt Redwood, and Weyerhauser timber companies, Grays Harbor County, Fort Lewis Army Base, L T Murray State Wildlife area, and numerous private land owners for access to recording sites. Any use of trade, product, or firm names is for descriptive purposes only and does not imply endorsement by the U.S. Government. The MT transfer function data inverted to produce the cross section models of this paper are available from the first author upon request.

References

Abers, G. A., L. S. MacKenzie, S. Rondenay, Z. Zhang, A. G. Wech, and K. C. Creager (2009), Imaging the source region of Cascadia tremor and intermediate-depth earthquakes, *Geology*, *37*, 1119–1122.

Allen, C. M., and C. G. Barnes (2006), Ages and some cryptic sources of Mesozoic plutonic rocks in the Klamath Mountains, California and Oregon, in *Geological studies in the Klamath Mountains province, California and Oregon: A Volume in Honor of William P. Irwin*, edited by A. W. Snoke and C. G. Barnes, *Geol. Soc. Am. Spec. Pap., 410*, 223–245.

Aprea, C., M. Unsworth, and J. Booker (1998), Resistivity structure of the Olympic Mountains and Puget Lowlands, *Geophys. Res. Lett.*, *25*, 1090–1112.

Ardia, P., M. M. Hirschmann, A. C. Withers, and T. J. Tenner (2012), H_2O storage capacity of olivine at 5–8 GPa and consequences for dehydration partial melting of the upper mantle, *Earth Planet. Sci. Lett.*, *345*, 104–116.

Aso, N., K. Ohta, and S. Ide (2013), Tectonic, volcanic, and semi-volcanic deep low-frequency earthquakes in western Japan, *Tectonophysics*, *600*, 27–40.

Audet, P., and R. Burgmann (2014), Possible control of subduction zone slow-earthquake periodicity by silica enrichment, *Nature*, *510*, 389–392.

Audet P., M. G. Bostock, N. I Christiansen, and S. M. Peacock (2010), Seismic evidence for overpressured subducted oceanic crust and megathrust fault sealing, *Nature*, *457*, 76–78.

Bedrosian, P.A., and S. E. Box (2007), Subsurface geometry of the Siletz-Klamath suture in southwest Oregon from magnetotelluric imaging, paper presented at Annual Meeting, Geological Society of America, Abstracts with programs, *39*(6), Denver, Colo.

Bedrosian, P. A., and D. W. Feucht (2014), Structure and tectonics of the northwestern United States from Earthscope USArray magnetotelluric data, *Earth Planet. Sci. Lett.*, *402*, 275–289, doi:10.1016/j.epsl/2013/07/035.

Bedrosian, P. A., M. J. Unsworth, G. D. Egbert, and C. H. Thurber (2004), Geophysical images of the creeping segment of the San Andreas Fault: Implications for the role of crustal fluids in the earthquake process, *Tectonophysics*, *385*, 137–156.

Beroza, G. C., and S. Ide (2011), Slow earthquakes and nonvolcanic tremor, *Annu. Rev. Earth Planet. Sci.*, *39*, 271–296.

Blakely, R. J., T. M. Brocher, and R. M. Wells (2005), Subduction zone magnetic anomalies and implications for hydrated forearc mantle, *Geology*, *33*, 445–448.

Blakely, R. J., B. L. Sherrod, C. S. Weaver, R. E. Wells, A. C. Rohay, E. A. Barnett, and N. E. Knepprath (2011), Connecting the Yakima fold and thrust belt to active faults in the Puget Lowland, Washington, *J. Geophys. Res.*, *116*, B07105, doi:10.1029/2010JB008091.

Booker, J. R., and A. D. Chave (1989), Introduction to the special issue on the EMSLAB-Juan de Fuca experiment, *J. Geophys. Res.*, *94*, 14,093–14,098.

Bostock, M. G. (2013), The Moho in subduction zones, *Tectonophysics*, *609*, 547–557.

Boyarko, D. C., and M. R. Brudzinski (2010), Spatial and temporal patterns of nonvolcanic tremor along the southern Cascadia subduction zone, *J. Geophys. Res.*, *115*, B00A22, doi:10.1029/2008JB006064.

Brasse, H., and D. Eydam (2008), Electrical conductivity beneath the Bolivian orocline and its relation to subduction processes at the South American continental margin, *J. Geophys. Res.*, *113*, B07109, doi:10.1029/2007JB005142.

Brudzinski, M. R., and R. M. Allen (2007), Segmentation in episodic tremor and slip all along Cascadia, *Geology*, *35*, 907–910.

Busby, C. J. (2013), Birth of a plate boundary at ca. 12 Ma in the Ancestral Cascades arc, Walker Lane belt of California and Nevada, *Geosphere*, *9*, 1147–1160.

Calvert, A. J., L. A. Preston, and A. M. Farahbod (2011), Sedimentary underplating at the Cascadia mantle-wedge corner revealed by seismic imaging, *Nat. Geosci.*, *4*, 545–548.

Clynne, M. A., and L. J. P. Muffler (2010), Geologic map of Lassen Volcanic National Park and vicinity, California, in *U. S. Geological Survey Science Investigation, Map, 2899*, 110 pp., U.S. Geological Survey, scale 1:50,000, Reston, Va.

Colgan, J. P., A. E. Egger, D. A. John, B. Cousens, R. J. Fleck, and C. D. Henry (2011), Oligocene and Miocene arc magmatism in northeastern California: Evidence for post-Eocene subduction segmentation of the subducting Farallon plate, *Geosphere*, *7*, 733–755.

Cox, S. F. (2005), Coupling between deformation, fluid pressures, and fluid flow in ore-producing hydrothermal systems at depth in the crust, *Soc. Econ. Geol. 100*, 39–75.

Cozzens, B. S., and G. A. Spinelli (2012), A wider seismogenic zone at Cascadia due to fluid circulation in subducting oceanic crust, *Geology*, *40*, 899–902.

Dickinson, W. R. (2008), Accretionary Mesozoic-Cenozoic expansion of the Cordilleran continental margin in California and adjacent Oregon, *Geosphere*, *4*, 329–353.
Dorsey, R. J., and T. A. LaMaskin (2007), Stratigraphic record of Triassic-Jurassic collisional tectonics in the Blue Mountains province, northeastern Oregon, *Am. J. Sci.*, *307*, 1167–1193.
duBray, E. A., and D. A. John (2011), Petrologic, tectonic, and metallogenic evolution of the Ancestral Cascades magmatic arc, Washington, Oregon, and northern California, *Geosphere*, *7*, 1102–1133.
DuRoss, C. B., R. J. Blakely, and R. E. Wells (2002), Cross sections through the Roseburg 30′ × 60′ quadrangle, Oregon: New constraints from potential field modeling, paper presented at *Cordilleran Section Annual Meeting*, Corvallis, Oreg.
Egbert, G. D., and J. R. Booker (1993), Imaging crustal structure in southwestern Washington with small magnetometer arrays, *J. Geophys. Res.*, *98*, 15,967–15,985.
Ernst, W. G. (2011), Accretion of the Franciscan complex attending Jurassic-Cretaceous geotectonic development of northern and central California, *Geol. Soc. Am. Bull.*, *123*, 1667–1678.
Evans, R. L., P. E. Wannamaker, R. S. McGary, and J. Elsenbeck (2014), Electrical structure of the central Cascadia subduction zone: the EMSLAB Lincoln line revisited, *Earth Planet. Sci. Lett.*, *402*, 265–274, doi:10.1016/j.epsl.2013.04.021.
Evans, W. C., R. H. Mariner, S. E. Ingebritsen, B. M. Kennedy, M. C. van Soest, and Mark A. Huebner (2001), Report of hydrologic investigations in the Three Sisters area of central Oregon, Summer 2001, *U.S. Geol. Surv. Water Resour. Invest. Rep., 02–4061*, 13 pp.
Faulds, J. E., and C. D. Henry (2008), Tectonic influences on the spatial and temporal evolution of the Walker Lane: An incipient transform fault along the evolving Pacific-North American plate boundary, in *Ores and Orogenesis: Circum-Pacific Tectonics, Geologic Evolution and Ore Deposits*, edited by J. E. Spencer, and S. R. Titley, *Ariz. Geol. Soc. Dig., 22*, 437–470.
Ferot, A., and N. Bolfan-Casanova (2012), Water storage capacity in olivine and pyroxene to 14 GPa: Implications for the water content of the Earth's upper mantle and nature of seismic discontinuities, *Earth Planet. Sci. Lett.*, *348*, 218–230.
Flueh, E. R., et al. (1998), New seismic images of the Cascadia subduction zone from cruise SO108–ORWELL, *Tectonophysics*, *293*, 69–84.
Frank, W. B., N. M. Shapiro, V. Kostoglodov, A. L. Husker, M. Campillo, J. S. Payero, and G. A. Prieto (2013), Low-frequency earthquakes in the Mexican Sweet Spot, *Geophys. Res. Lett.*, *40*, 2661–2666, doi:10.1002/grl.50561.
Frost, B. R., and K. Bucher (1994), Is water responsible for geophysical anomalies in the deep continental crust?: A petrological perspective, *Tectonophysics*, *231*, 293–309.
Furukawa, Y. (2009), Convergence of aqueous fluid at the corner of the mantle wedge: Implications for a generation mechanism of deep low-frequency earthquakes, *Tectonophysics*, *469*, 85–92.
Gao, H., and Y. Shen (2014), Upper mantle structure of the Cascades from full-wave ambient noise topography: Evidence for 3D mantle upwelling in the back-arc, *Earth. Planet. Sci. Lett.*, *390*, 222–233.
Gomberg, J., the Cascadia 2007, and Beyond Working Group (2010), Slow-slip phenomena in Cascadia from 2007 and beyond: A review, *Geol. Soc. Am. Bull.*, *122*, 963–978.
Grant, F. S., and G. F. West (1965), *Interpretation Theory in Applied Geophysics*, 584 pp., McGraw-Hill, N. Y.
Grove, T. L., C. B. Till, and M. J. Krawcynski (2012), The role of H_2O in subduction zone magmatism, *Annu. Rev. Earth Planet. Sci.*, *40*, 413–439.
Gulick, S. P. S., A. M. Meltzer, and S. H. Clarke, Jr. (1998), Seismic structure of the southern Cascadia subduction zone and accretionary prism north of the Mendocino triple junction, *J. Geophys. Res.*, *103*, 27,207–27,222.
Guo, X., Y. Yoshino, and I. Katayama (2011), Electrical conductivity anisotropy of deformed talc rocks and serpentinites at 3 GPa, *Phys. Earth Planet. Inter.*, *188*, 69–81.
Hasterok, D., D. S. Chapman, and E. E. Davis (2011), Oceanic heat flow: Implications for global heat loss, *Earth Planet. Sci. Lett.*, *311*, 386–396.
Heise, W., T. G. Caldwell, E. A. Bertrand, G. J. Hill, S. L. Bennie, and Y. Ogawa (2013), Changes in electrical resistivity track changes in tectonic plate coupling, *Geophys. Res. Lett.*, *40*, 5029–5033, doi:10.1002/grl50959.
Hildreth, W. (2007), Quaternary magmatism in the Cascades: Geologic perspectives, *U.S. Geol. Surv. Prof. Pap. 1744*, 125 pp.
Hill, G. J., T. G. Caldwell, W. Heise, D. G. Chertkoff, H. M. Bibby, M. K. Burgess, J. P. Cull, and R. A. F. Cass (2009), Distribution of melt beneath Mount St Helens and Mount Adams inferred from magnetotelluric data, *Nat. Geosci.*, *2*, 785–789.
Humphreys, E. D. (2008), Cenozoic slab windows beneath the western United States, in *Ores and Orogenesis: Circum-Pacific Tectonics, Geologic Evolution and Ore Deposits*, edited by J. E. Spencer and S. R. Titley, *Ariz. Geol. Soc. Dig., 22*, 389–396.
Hurwitz, S., R. H. Mariner, U. Fehn, and G. T. Snyder (2005), Systematics of halogens and their radioisotopes in thermal springs of the Cascade Range, central Oregon, western USA, *Earth Planet. Sci. Lett.*, *235*, 700–714.
Husker, A. L., V. Kostoglodov, V. M. Cruz-Atienza, D. Legrand, N. M. Shapiro, J. S. Apyero, M. Campillo, and E. Huesca-Perez (2012), Temporal variations of non-volcanic tremor (NVT) locations in the Mexican subduction zone: Finding the NVT sweet spot, *Geochem. Geophys. Geosyst.*, *13*, Q03011, doi:10.1029/2011GC003916.
Hyndman, R. D. (1988), Dipping seismic reflectors, electrically conductive zones, and trapped water in the crust over a subducting plate, *J. Geophys. Res.*, *93*, 13,391–13,405.
Hyndman, R. D. (2013), Downdip landward limit of Cascadia great earthquake rupture, *J. Geophys. Res.*, *118*, 5530–5549, doi:10.1002/jgrb.50390.
Hyndman, R. D., and C. A. Currie (2011), Why is the North America Cordillera so high? Hot backarcs, thermal isostasy, and mountain belts, *Geology*, *39*, 783–786.
Hyndman, R. D., L. L. Vanyan, G. Marquis, and L. K. Law (1993), The origin of electrically conductive lower continental crust: saline water or graphite?, *Phys. Earth Planet. Inter.*, *81*, 325–344.
Hyndman, R. D., C. A. Currie, and S. P. Mazzotti (2005), Subduction zone backarcs, mobile belts, and orogenic heat, *GSA Today*, *15*, 4–10.
Ingebritsen, S. E., and R. H. Mariner (2010), Hydrothermal heat discharge in the Cascade Range, northwestern United States, *J. Volcanol. Geotherm. Res.*, *196*, 208–218.
Ikemoto, A., and H. Iwamori (2014), Numerical modeling of trace element transportation in subduction zones: Implications for geofluid processes, *Earth Planet. Space*, *66*, 26.
Ito, E., D. M. Harris, and A. T. Anderson (1983), Alteration of oceanic crust and geologic cycling of chlorine and water, *Geochem. Cosmochem. Acta*, *47*, 1613–1624.
Ito, Y., et al. (2013), Episodic slow slip events in the Japan subduction zone before the 2011 Tohoku-Oki earthquake, *Tectonophysics*, *600*, 14–26.
Jodicke, H., A. Jording, L. Ferrari, J. Arzate, K. Mezger and L. Rupke (2006), Fluid release from the subducted Cocos plate and partial melting of the crust deduced from magnetotelluric studies in southern Mexico: Implications for the generation of volcanism and subduction dynamics, *J. Geophys. Res.*, *111*, B08102, doi:10.1029/2005JB003739.

Kanda, W., and Y. Ogawa (2014), Three-dimensional electromagnetic imaging of fluids and melts beneath the NE Japan arc revisited by using geomagnetic transfer function data, *Earth Planet. Space*, *66*, doi:10.1186/1880-5981-66-39, 8.
Kato, A., A. Saiga, T. Takeda, T. Iwasaki, and T. Matsuzawa (2014), Non-volcanic seismic swarm and fluid transportation driven by subduction of the Philipping Sea slab beneath the Kii Peninsula, Japan, *Earth Planet. Space*, *66*, doi:10.1186/1880-5981-66-86, 8.
Kawamoto, T., K. Mibe, H. Bureau, S. Reguer, C. Mocuta, S. Kubsky, D. Thiaudiere, S. Ono, and T. Kogiso (2014), Large-ion lithophile elements delivered by saline fluids to the sub-arc mantle, *Earth Planet. Space*, *66*, doi:10.1186/1880-5981-66-61, 11.
Kohlstedt, D. L., and B. K. Holtzman (2009), Shearing melt out of the Earth: An experimentalist's perspective on the influence of deformation on melt extraction, *Annu. Rev. Earth Planet. Sci.*, *37*, 561–593.
Kurtz, R. D., J. M. deLaurier, and J. C. Gupta (1986) A magnetotelluric sounding across Vancouver Island detects the subducting Juan de Fuca plate, *Nature*, *321*, 596–599.
Kurtz, R. D., J. M. deLaurier, and J. C. Gupta (1990), The electrical conductivity distribution beneath Vancouver Island: A region of active plate subduction, *J. Geophys. Res.*, *95*, 10,929–10,946.
Kusuda, C., H. Iwamori, H. Nakamura, K. Kazahaya, and N. Morikawa, (2014), Arima hot spring waters as a deep-seated brine from subducting slab, *Earth Planet. Space*, *66*, doi:10.1186/1880-5981-66-119, 13.
Ledo, J., and A. G. Jones (2001), Regional electrical resistivity structure of the southern Canadian Cordillera and its physical interpretation, *J. Geophys. Res.*, *106*, 30,755–30,769.
Leeman, W. P., J. F. Lewis, R. C. Evarts, R. M. Conrey, and M. J. Streck (2005), Petrologic constraints on the thermal structure of the Cascades arc, *J. Volcanol. Geotherm. Res.*, *140*, 67–105.
Liu, K., A. Levander, Y. Zhai, R. W. Porritt, and R. M. Allen (2012), Asthenospheric flow and lithospheric evolution near the Mendocino triple junction, *Earth Planet. Sci. Lett.*, *323–324*, 60–71.
McCaffrey, R., R. W. King, S. J. Payne, and M. Lancaster (2013), Active tectonics of northwestern U.S. inferred from GPS-derived surface velocities, *J. Geophys. Res.*, *118*, 709–723, doi:10.1029/2012JB009473.
McCrory, P. A., and D. S. Wilson (2013), A kinematic model for the formation of the Siletz-Crescent forearc terrane by capture of coherent fragments of the Farallon and Resurrection plates, *Tectonics*, *32*, 718–736, doi:10.1002/tect.20045.
McCrory, P. A., J. L. Blair, F. Waldhauser, and D. H. Oppenheimer (2012), Juan de Fuca slab geometry and its relation to Wadati-Benioff zone seismicity, *J. Geophys. Res.*, *117*, B09306, doi:10.1029/2012JB009407.
McCrory, P. A., R. D. Hyndman, and J. L. Blair (2014), Relationship between the Cascadia fore-arc mantle wedge, non-volcanic tremor, and the downdip limit of seismogenic rupture, *Geochem. Geophys. Geosyst.*, *15*, 1071–1095, doi.10.1002/2013GC005144.
McGary, R. S., R. L. Evans, P. E. Wannamaker, J. Elsenbeck, and S. Rondenay (2014), Subducting slab to surface pathway for melt and fluids beneath Mount Rainier, *Nature*, *511*, 338–341.
McLaughlin, R. J., S. A. Kling, R. Z. Poore, K. McDougall, and E. D. Beutner (1982), Post-middle Miocene accretion of Franciscan rocks, northwestern California, *Geol. Soc. Am. Bull.*, *93*(7), 595–605.
McLaughlin, R. J., S. D. Ellen, M. C. Blake, Jr., A. S. Jayko, W. P. Irwin, K. R. Aalto, G. A. Carver, and S. H. Clarke, Jr. (2000), Geology of the Cape Mendocino, Eureka, Garberville, and southwestern part of the Hayfork 30 × 60 minute quadrangles and adjacent offshore area, northern California, *U.S. Geol. Surv. Misc. Field Stud. Map., MF-2336*, 26 pp (6 sheets).
McNeill, L. C., J. Geersen, J. Springett, A. M. Trehu, and D. J. Wilson (2013), Sediment flux and accretion history on the Cascadia and Sumatra margins, Abstract T511-05 presented at 2013 Fall Meeting, AGU, San Francisco, Calif.
Meqbel, N. M., G. D. Egbert, P. E. Wannamaker, A. Kelbert, and A. Schultz (2014), Deep electrical resistivity structure of the Pacific NW derived from 3-D inversion of Earthscope USArray magnetotelluric data, *Earth Planet. Sci. Lett.*, *402*, 290–304, doi:10.1016/j.epsl.2013.12.026.
Monger, J., and R. Price (2002), The Canadian Cordilleran: Geology and tectonic evolution, *Can. Soc. Explor. Geophys. Recor.*, February, 17–36.
Monger, J. W. H., P. van der Heyden, J. M. Journeay, C. A. Evenchick, and J. B. Mahoney (1994), Jurassic-Cretaceous basin along the Canadian Coastal belt: their bearing on pre-mid-Cretaceous sinistral developments, *Geology*, *22*, 175–178.
Muffler, L. J. P., M. A. Clynne, A. T. Calvert, and D. E. Champion (2011), Diverse, discrete, mantle-derived batches of basalt erupted along a short normal fault zone: The Poison Lake chain, southernmost Cascades, *Geol. Soc. Am. Bull.*, *123*, 2177–2200.
Ni, H., H. Keppler, and H. Behrens (2011), Electrical conductivity of hydrous basaltic melts: Implications for partial melting in the upper mantle, *Contrib. Mineral. Petrol.*, *162*, 637–650, doi:10.1007/s00410-011-0617-4.
Nesbitt, B. (1993), Electrical resistivities of crustal fluids, *J. Geophys. Res.*, *98*, 4301–4310.
Ogawa, Y., and Y. Honkura (2004), Mid-crustal electrical conductors and their correlations to seismicity and deformation at Itoigawa-Shizuoka tectonic line, central Japan, *Earth Planet. Space*, *56*, 1285–1291.
Park, S. K., and L. C. Ostos (2013), Constraints from magnetotelluric measurements on magmatic processes and upper mantle structure in the vicinity of Lassen volcanic center, northern California, *Geosphere*, *9*, 382–393.
Parsons, T., et al. (1995), Crustal structure of the Cascadia fore arc of Washington, *U.S. Geol. Surv. Prof. Pap., 1661-D*, 40 pp.
Peacock, S. M. (2009), Thermal and metamorphic environment of subduction zone episodic tremor and slip, *J. Geophys. Res.*, *114*, B00A07, doi:10.1029/2008JB005978.
Pommier, A. (2014), Geophysical assessment of migration and storage conditions of fluids in subduction zones, *Earth, Planet. Space*, *66*, 38.
Prohoroff, R., J. Wakabayashi, and T. A. Dumitru (2012), Sandstone matrix olistostrome deposited on intra-subduction complex serpentinite, Franciscan Complex, western Marin County, California, *Tectonophysics*, *568*, 296–305.
Ramachandran, K., R. D. Hyndman, and T. M. Brocher (2006), Regional P wave velocity structure of the northern Cascadia subduction zone, *J. Geophys. Res.*, *111*, B12301, doi:10.1029/2005JB004108.
Reynard, B., K. Mibe, and B. Van de Moortele (2011), Electrical conductivity of the serpentinised mantle and fluid flow in subduction zones, *Earth Planet. Sci. Lett.*, *307*, 387–394.
Rippe, D., M. J. Unsworth, and C. A. Currie (2013), Magnetotelluric constraints on the fluid content in the upper mantle beneath the southern Canadian Cordillera: Implications for rheology, *J. Geophys. Res.*, *118*, 1–24, doi:10.1002/jgrb.50255.
Rondenay, S., M. G. Bostock, and J. Shragge (2001), Multiparameter two-dimensional inversion of scattered teleseismic body waves 3. Application to the Cascadia 1993 data set, *J. Geophys. Res.*, *106*, 30,795–30,807.
Rondenay, S., G. A. Abers, and P. E. van Keken (2008), Seismic imaging of subduction zone metamorphism, *Geology*, *36*, 275–278.
Royer, A. A., and M. G. Bostock (2014), A comparative study of low frequency earthquake templates in northern Cascadia, *Earth Planet. Sci. Lett.*, *420*, 247–256, doi:10.1016/j.epsl.08.040.
Saffer, D. M., and H. J. Tobin (2011), Hydrogeology and mechanics of subduction zone forearcs: Fluid flow and pore pressure, *Annu. Rev. Earth Planet. Sci.*, *39*, 157–186.

Schmalzle, G. M., R. McCaffrey, and K. C. Creager (2014), Central Cascadia subduction zone creep, *Geochem. Geophys. Geosyst.*, *15*, 1515–1532, doi:10.1002/2013GC005172.
Schmidt, M. E., A. L. Grunder, and M. C. Rowe (2008), Segmentation of the Cascade arc as indicated by Sr and Nd isotopic variation among diverse primitive basalts, *Earth Planet. Sci. Lett.*, *266*, 166–181.
Sibson, R. (2007), Au-quartz mineralization near the base of the continental seismogenic zone, in *Deformation of the Continental Crust: The Legacy of Mike Coward, Geol. Soc. London Spec. Publ.*, *272*, 519–532.
Snavely, P. D., Jr. (1987), Tertiary geologic framework, neotectonics, petroleum potential of the Oregon-Washington continental margin, in Geology and resources potential of the continental margin of western North America and adjacent ocean basins: Beaufort Sea to Baja California, in *Circum-Pacific Council for Energy and Mineral Resources, Earth Sci. Ser.*, vol. 6, edited by D. W. Scholl, A. Grantz, and J. G. Vedder, Ch. 14, American Assoc. of Petrol. Geol., Houston, pp. 305–335.
Soyer, W., and M. Unsworth (2006), Deep electrical structure of the northern Cascadia (British Columbia, Canada) subduction zone: Implications for the distributions of fluids, *Geology*, *34*, 53–56.
Stanley, W. D., W. D. Mooney, and G. S. Fuis (1990), Deep crustal structure of the Cascade Range and surrounding regions from seismic refraction and magnetotelluric data, *J. Geophys. Res.*, *95*, 19,419–19,438.
Stanley, W. D., S. Y. Johnson, A. Y. Qamar, C. S. Weaver, and J. M. Williams (1996), Tectonics and seismicity of the southwest Washington Cascade Range, *Bull. Seismol. Soc. Am.*, *86*, 1–18.
Stewart, J. H., and J. E. Carlson (1978), *Geologic Map of Nevada*, U.S. Geological Survey and Nevada Bureau of Mines and Geology, 1:500000, two sheets, Reston, Va.
Syracuse, E. M., P. E. van Keken, and G. A. Abers (2010), The global range of subduction zone thermal models, *Phys. Earth Planet. Inter.*, *183*, 73–90.
Thomas, A., M. Bostock, A. Plourde, and P. Audet (2013), Low-frequency earthquakes in central and southern Cascadia, Abstract T41A-2564 presented at 2013 Annual Meeting, AGU, San Francisco, Calif.
Thurber, C., H. Zhang, T. Brocher, and V. Langenheim (2009), Regional three-dimensional seismic velocity model of the crust and uppermost mantle of northern California, *J. Geophys. Res.*, *114*, B01304, doi:10.1029/2008JB005766.
Till, C. B., T. L. Grove, R. W. Carlson, M. J. Fouch, J. M. Donnelly-Nolan, L. S. Wagner, and W. K. Hart (2013), Depths and temperatures of $<$10.5 Ma mantle melting and the lithosphere-asthenosphere boundary below southern Oregon and northern California, *Geochem. Geophys. Geosyst.*, *14*, 864–879.
Trehu, A., M., R. J. Blakely, and M. C. Williams (2012), Subducted seamounts and recent earthquakes beneath the central Cascadia forearc, *Geology*, *40*, 103–106.
Tullis, J., R. A. Yund, and J. Farver (1996), Deformation enhanced fluid distribution in feldspar aggregates and implications for ductile shear zones, *Geology*, *24*, 63–66.
Umeda, K., Y. Ogawa, K. Asamori, and T. Oikawa (2006), Aqueous fluids derived from a subducting slab: observed high ^{3}He and conductive anomaly in a non-volcanic region, Kii Peninsula, southwest Japan, *J. Volcanol. Geotherm. Res.*, *149*, 47–61.
Van Keken, P. E., B. R. Hacker, E. M. Syracuse, and G. A. Abers (2011), Subduction factory: 4. Depth-dependent flux of H_2O from subducting slabs worldwide, *J. Geophys. Res.*, *116*, B01401, doi:10.1029/2010JB007922.
Van Soest, M., B. M Kennedy, W. C. Evans, and R. H. Mariner (2002), Mantle helium and carbon isotopes in Separation Creek geothermal springs, Three Sisters area, central Oregon: Evidence for renewed volcanic activity or a long term steady state system?, *Geotherm. Resour. Council Trans.*, *26*, 361–366.
Vidale, J. E., D. A. Schmidt, S. D. Malone, A. J. Hotovec-Ellis, S. C. Moran, K. C. Creager, and H. Houston (2014), Deep long-period earthquakes west of the volcanic arc in Oregon: evidence of serpentine dehydration in the fore-arc mantle wedge, *Geophys. Res. Lett.*, *41*, 370–376, doi:10.1002/2013GL059118.
Wada, I., and K. Wang (2009), Common depth of slab-mantle decoupling: reconciling diversity and uniformity of subduction zones, *Geochem. Geophys. Geosyst.*, *10*, Q10009, doi:10.1029/2009GC002570.
Wallace, L. M., J. Beavan, S. Bannister, and C. Williams (2012), Simultaneous long-term and short-term slow slip events at the Hikurangi subduction margin, New Zealand: Implications for processes that control slow slip event occurrences, duration and migration, *J. Geophys. Res.*, *117*, B11402, doi:10.1029/2012JB009489.
Wannamaker, P. E. (2000), Comment on "The petrological case for a dry lower crust" by Bruce W. D. Yardley and John W. Valley, *J. Geophys. Res.*, *105*, 6057–6065.
Wannamaker, P. E., J. R. Booker, A. G. Jones, A. D. Chave, J. H. Filloux, H. S. Waff, and L. K. Law (1989), Resistivity cross-section through the Juan de Fuca subduction system and its tectonic implications, *J. Geophys. Res.*, *94*, 14,127–14,144.
Wannamaker, P. E., D. P. Hasterok, J. M. Johnston, J. A. Stodt, D. B. Hall, T. L. Sodergren, L. Pellerin, V. Maris, W. M. Doerner, and M. J. Unsworth (2008), Lithospheric dismemberment and magmatic processes of the Great Basin-Colorado Plateau transition, Utah, implied from magnetotellurics, *Geochem. Geophys. Geosyst.*, *9*, Q05019, doi:10.1029/2007GC001886.
Wannamaker, P. E., T. G. Caldwell, G. R. Jiracek, V. Maris, G. J. Hill, Y. Ogawa, H. M. Bibby, S. L. Bennie, and W. Heise (2009), Fluid and deformation regime of an advancing subduction system at Marlborough, New Zealand, *Nature*, *460*, 733–736, doi:10.1038/nature08204.
Wech, A. G., K. C. Creager, and T. I. Melbourne (2009), Seismic and geodetic constraints on Cascadia slow slip, *J. Geophys. Res.*, *114*, B10316, doi:10.1029/2008JB006090.
Wells, R. E., and R. McCaffrey (2013), Steady rotation of the Cascade arc, *Geology*, *41*, 1027–1030.
Wells, R. E., A. S. Jayko, A. R. Niem, G. Black, T. Wiley, E. Baldwin, K. M. Molenaar, K. L. Wheeler, C. B. DuRoss, and R. W. Givler (2000) Geologic map and database of the Roseburg 30 $\times$ 60′ quadrangle, Douglas and Coos counties Oregon, *U. S. Geol. Surv. Open File Rep. 00–376*.
Wells, R. E., D. Bukry, R. Friedman, D. Pyle, R. Duncan, P. Haeussler, and J. Wooden (2014), Geologic history of Siletzia, a large igneous province in the Oregon and Washington Coast Range: correlation to the geomagnetic polarity time scale and implications for a long-lived Yellowstone hotspot, *Geosphere*, *10*(4), 679–719, doi:10.1130/GES01018.1.
Wilson, D. S., P. A. McCrory, and R. G. Stanley (2005), Implications of volcanism in coastal California for the deformation history of western North America, *Tectonics*, *24*, TC3008, doi:10.1029/2003TC001621.
Worzewski, T., M. Jegen, H. Kopp, H. Brasse, and W. T. Castillo (2011), Magnetotelluric image of the fluid cycle in the Costa Rican subduction zone, *Nat. Geosci.*, *4*, 108–111.
Wright, J. E., and S. J. Wyld (2006), Gondwanan, Iapetan, Cordilleran interactions: A geodynamic model for the Paleozoic tectonic evolution of the North American Cordillera, in *Paleogeography of the North American Cordillera: Evidence for and Against Large-Scale Displacements*, edited by J. W. Haggart, R. J. Enkin, and J. W. H. Monger, *Geol. Assoc. Can. Spec. Pap., 46*, 377–408.
Yoshino, T., and T. Katsura (2013), Electrical conductivity of mantle minerals: Role of water in conductivity anomalies, *Annu. Rev. Earth Planet. Sci.*, *41*, 605–628.